Chapter 5

Evolution of a Late Precambrian Carbonate Platform, Buah Formation and Ara Group, Sultanate of Oman

Kristin D. Bergmann[1], John P. Grotzinger[1], Magdalena Osburn[1], Jena Johnson[1], Gideon Lopes Cardozo[2], Timothy Lyons[3], Alexandra Ruiz[3], Steven Bates[3]

[1]California Institute of Technology

[2]Petroleum Development Oman

[3]University of California, Riverside

5.1 Abstract

The late Precambrian to earliest Cambrian Huqf Supergroup of Oman preserves a detailed record of sedimentation just preceding and during early animal evolution and diversification. Currently, the post-Shuram Formation carbonates that capture the transition into the Cambrian—from the recovery from the extreme negative Shuram carbon isotope excursion to the Precambrian-Cambrian Boundary—have competing models for correlation across Oman, which affects interpretations of isotopic signals, depositional models and environmental reconstructions. We employ an integrated approach to address the question of correlation and develop

a new depositional model for the Oman stratigraphy that captures this critical time interval. We characterize lithofacies and lithofacies associations within measured outcrop sections and in subsurface cores. From these observations, we build a sequence stratigraphic framework for the microbial carbonate strata exposed in Central Oman and the Oman Mountains using lithofacies stacking patterns and key surfaces. Results from this work include $\sim$ 3000 meters of logged outcrop stratigraphy, $\sim$ 300 meters of logged subsurface cores and geologic mapping of the large-scale sequences preserved in the carbonate strata. Additionally, isotopic measurements of δ^{13}C, δ^{18}O, and $\delta^{34}S_{CAS}$ were made and interpreted within the context of our regional sequence stratigraphic model to examine the potential for spatial variability in the proxies. The δ^{13}C variability in these carbonates is temporally significant and suggests a link between the carbon cycle and carbonate platform cyclicity. The $\delta^{34}S_{CAS}$ record is also temporally significant but the absolute magnitude of enrichment appears spatially variable. Our complimentary field observations and isotopic data suggest early interpretations were correct that the bulk of the stratigraphy in central Oman can be correlated with the Buah Formation in the Oman Mountains and subsurface but there is also a potential outcrop equivalent of the Ara Group in central Oman. The interval leading up to the Precambrian-Cambrian boundary is exceptionally preserved in the subsurface and outcrops of Oman and here we provide a new unified framework for correlation of the stratigraphy and chemostratigraphy throughout Oman.

5.2 Introduction

The Huqf Supergroup of Oman was deposited between $\sim$ 720 and 520 Ma from late Precambrian into earliest Cambrian time [1]. As such it preserves a detailed record of environmental conditions during early animal evolution and diversification (Fig. 5.1). The Huqf Supergroup is subdivided into the Abu Mahara, Nafun and Ara Groups [1, 2](Fig. 5.1).

The latest Precambrian to Cambrian strata of the Buah Formation within the Nafun Group and overlying Ara Group currently have competing models for correlation across Oman which affects environmental reconstruction during this critical interval of animal evolution [3, 4, 5]. This is likely due in part to rapidly changing topography associated with the onset of rifting during the latest Precambrian [6, 7]. Regional studies have relied on absolute age dates, sedimentology and chemostratigraphy for correlation between subsurface deposits, the Huqf outcrop area in Central Oman and the Oman Mountains [1, 8, 9, 4]. However, facies heterogeneities, sparse age constraints, a limited fossil record and complex topography have hampered lateral correlation. Previous work on the carbonates exposed in central Oman has resulted in two competing regional models for correlation of the late Precambrian stratigraphy [10, 8, 11, 9, 4].

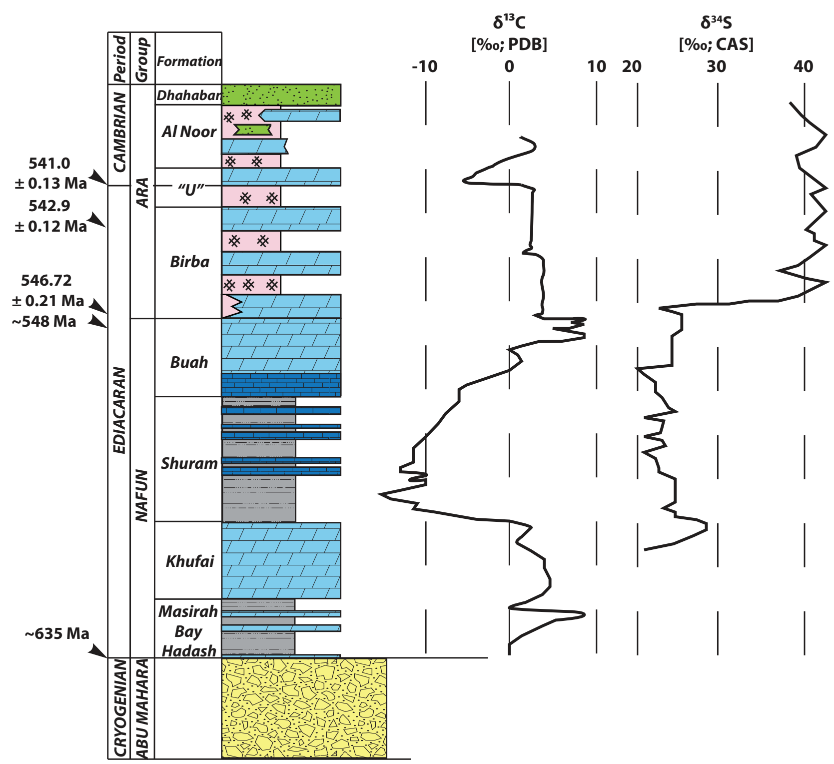

Figure 5.1: Generalized Stratigraphy and previously proposed chemostratigraphic model for the Huqf Supergroup.

Generalized chemostratigraphic model from [9], Absolute age constraints from Oman [1]

Early mappers and stratigraphers suggested the strata preserved in Central Oman were equivalent to the Buah Formation carbonates in the Oman Mountains (termed the Kharus Formation by early workers) [8, 12, 13, 14]. Since 2000, some researchers have contended that the strata in Central Oman preserve both the Buah Formation and the Ara Group [10, 11, 15] and recent work has suggested the strata include the A4 carbonate recording the Precambrian-Cambrian boundary [4, 5](Fig. 5.2). These researchers have divided the stratigraphy into a 'Buah Formation' and a newly named 'Sirab Formation' [4, 5]. The recently named Sirab Formation from the Huqf outcrop area, previously termed the Upper Buah Formation [8], was divided into four members (Ramayli, Salutiyyat, Shital and Aswad) [4, 5]. The Ramayli Member is correlated with the A4C and the Shital and Aswad Members are thought to be Cambrian in age [4, 5]. However, the temporal change in the $\delta^{34}S_{CAS}$ in carbonates from Southern Oman from values of $\sim +20‰$ in the Nafun Group to values $\sim +30$–$40‰$ in the Ara Group of the SOSB, have led others to challenge this correlation scheme [9]. The $\delta^{34}S$ isotopic excursion in the Ara Group is consistent with enriched values measured in $\delta^{34}S_{CAS}$ and $\delta^{34}S_{SO4}$ from rocks of the latest Precambrian to Cambrian age globally including India, China, Iran and Siberia [16, 17, 18, 19, 20, 21].

In light of the ongoing uncertainties with these deposits and the importance of regional correlation during the latest Precambrian, this study has three goals:

1. Develop a sequence stratigraphic model for the thick sequence of carbonates post-dating the Shuram Formation in three locations: the Central Oman Huqf outcrop area, the Oman Mountains and the subsurface, including Ara-equivalent Birba Platform carbonates found on the Eastern Flank of the South Oman Salt Basin (SOSB), which lack evaporites. Our methods include bed-by-bed lithofacies characterization, identifying lithofacies associations, creating a depositional model and characterizing stacking patterns at all scales.

2. Complete detailed outcrop gamma ray logging of the entire Nafun Group to improve correlation to the subsurface.

3. Test the usefulness of $\delta^{13}C$ and $\delta^{34}S$ isotopic records as a correlation tool

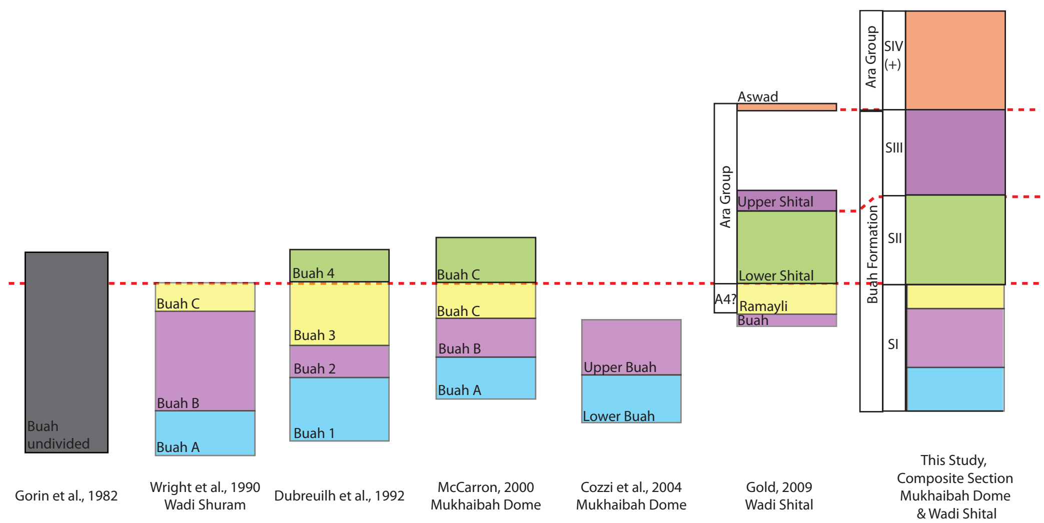

Figure 5.2: Previous stratigraphic divisions of the Buah and Sirab Formations in the Huqf Outcrop Area. Early workers mapped all stratigraphy exposed in the Huqf Outcrop Area as Buah Formation. Later workers divided the stratigraphy into two formations—the Buah and Sirab.

by comparing the isotopic measurements to the sequence stratigraphic model.

5.3 Geologic setting

The Precambrian stratigraphy in Oman begins with the Abu Mahara Group (ca. 725–$<$ 645 Ma) which includes thick successions of two glacial diamictites and interglacial mudstones, siltstones and sandstones [22, 23, 24]. The second glacial deposit, correlated with the Marinoan Glaciation ($\sim$ 635 Ma), is capped by the Hadash cap carbonate [22, 1]. The Nafun Group, which overlies the Abu Mahara Group, is composed of two large siliciclastic-to-carbonate cycles [13, 12, 8, 2]. The lower cycle includes the Masirah Bay Formation, composed of sandstones and siltstones and the Khufai Formation, a shallowing-upward prograding carbonate platform with a ramp morphology [25, 13, 12, 8, 26]. The upper cycle includes the Shuram Formation, composed of hummocky cross-stratified siltstone and oolitic grainstone and the Buah Formation, a shallowing upward carbonate platform [27, 28, 13, 12, 11, 15, 8]. The Nafun Group is capped by the Ara Group in the subsurface which is composed of carbonate-evaporite cycles and hosts proven oil reserves [6, 7, 29, 30]. This contact is demonstrably unconformable in the subsurface Northern Carbonate Domain [6].

Absolute age constraints on Precambrian stratigraphy can be a challenge; however, multiple high-resolution U/Pb dates from the Huqf Supergroup exist [1]. An age date from the Gubrah Formation in Abu Mahara Group of 711.52 ± 0.20 Ma helps constrain the Sturtian glaciation [1]. No absolute age dates have yet to be reported from the Nafun Group. Various ash beds from the South Oman Salt basin help constrain the age and rate of deposition of the Ara Group. The A0 contains an ash bed with an age of 546.72 ± 0.21 Ma, the A3 contains two ash beds with ages 542.90 ± 0.12 Ma and 542.33 ± 0.12 Ma, and the A4 contains an ash bed with an age of 541.00 ± 0.13 Ma [1]. The ash bed in the A4 carbonate provides a key age constraint on a -4‰ δ^{13}C excursion that has been correlated with the Precambrian-Cambrian boundary globally [1, 30, 31, 32, 33]. Ages from zircons sampled from ignimbrites of the Fara Formation in the Oman Mountains suggest it is broadly time equivalent to the Ara Group (542. 54 ± 0.45, 545.94 ± 0.68, 548.3 ± 0.8 [1]. All ages are ^{206}Pb/^{238}U from CA-TIMS analysis on individual zircons [1].

Because of poor age constraints, chemostratigraphy of carbonates has been used extensively for correlation in the Neoproterozoic (eg., [34, 35, 36, 37, 32]). Within the Nafun Group (ca. 645-547 Ma), the enigmatic Shuram negative carbon isotope excursion begins in the Upper Khufai Formation, declines to values of ∼ -12‰ $\delta^{13}C_{min}$ VPDB in the Shuram Formation before recovering in the Buah Formation [38, 8, 11, 15, 39, 27, 28, 40, 41](Fig. 5.1). The Upper Buah Formation in well 'MQ1' contains a positive isotope excursion that has been correlated with a positive carbon isotope excursion (+5 - 6‰) dated at 548.8 ± 1 Ma from the Nama Group of Namibia [42, 43, 39, 31]. The Precambrian-Cambrian boundary in Oman is characterized by a negative carbon isotope anomaly (∼ -4‰ $\delta^{13}C_{min}$ PDB) and water column anoxia/euxinia in basinal environments [44, 29, 45, 30, 1]. The Ara Group in the SOSB contains higher $\delta^{34}S_{CAS}$ (∼ 40‰) than the underlying Nafun group ($\sim 20‰$) (Fig. 5.1) [39, 9, 3, 46].

The record of early animal evolution from Oman includes biomarker evidence for eukaryotic sponges (Demospongiae) from the Abu Mahara Group onwards as well as abundant bacteria and chlorophyte microalgae primary producers [47]. The Ara Group includes both *Cloudina* and *Namacalathas*, early calcifying organisms, both of which appear to go extinct in the A4C member [44]. However, unlike most other late Precambrian records, the Huqf Supergroup does not contain abundant macroscopic Ediacaran fauna. Instead, the Nafun and Ara Groups are dominated by microbially-influenced carbonates including a variety of stromatolite morphologies, crinkly laminite and thrombolite facies [8, 11, 30, 4, 5].

5.4 Methods

5.4.1 Sedimentology and stratigraphy

Outcrop sections and subsurface cores were logged during 2011-2013. Five long sections and nine shorter sections were logged in the Huqf outcrop area of the Buah and Sirab formations. Three long sections of the Buah Formation were logged in the Oman Mountains. Additionally cored intervals of 10 subsurface wells were logged. Grain size, carbonate texture using the Dunham classification system, lithology, sedimentary structures, and key components were recorded for each log. Logged sections were digitized into excel. A lithofacies scheme was developed to account for the full variability in lithofacies seen from the subsurface to outcrop areas. Thin sections were manufactured from rock samples collected in the field and from subsurface cores to supplement lithofacies descriptions. A sequence stratigraphic scheme for the outcrop sections was developed using vertical lithofacies stacking patterns, key surfaces and changes in lithofacies associations with stratigraphic height.

A geologic map of the major sequences identified in the Buah and Sirab formations was generated for the Huqf outcrop area. GPS control points of field observations were used in conjunction with Quickbird satellite imagery to build the geologic map. A revised structural map of the Buah Formation in Wadi Bani Awf and Wadi Hajir in the Oman Mountains was also developed from field observations and Quickbird satellite imagery.

5.4.2 Gamma ray logging

An outcrop spectral gamma ray survey was completed on the entire Nafun Group in the Huqf outcrop area using a portable RS-125 Super-SPEC by Radiation Solutions. The handheld instrument uses a large NaI crystal detector (103 cm^3) to detect total bulk-GR, potassium (K), uranium (U) and thorium (Th). We used a 60 second count time and measured each section at a 1 meter interval. Two complete sections of the Khufai Formation, one composite section of the Shuram Formation and five composite sections of the Buah and Sirab formations were logged.

5.4.3 Carbon and oxygen isotope analysis

Carbon and oxygen isotopic analysis was the completed on eight of the outcrop sections at a 2 meter sampling interval and on six subsurface wells. The majority of the $\delta^{13}C$ and $\delta^{18}O$ data was analyzed at the California Institute of Technology on a ThermoFinnigan Delta V Plus attached to a ThermoFinnigan GasBench II. For the samples analyzed at Caltech, approximately 300 μg of carbonate were weighed into gas vials, flushed with UHP He for 5 minutes and reacted with 100% H_3PO_4 at 78°C for 1 hour within the ThermoFinnigan GasBench II. Three standards were run at the beginning of an 88 sample run and then 8 unknown samples were bracketed by 1 standard. Standard reproducibility was better than 0.5‰ in $\delta^{13}C$ for two in-house standards and better than 0.35‰ and 0.5‰ for $\delta^{18}O$ for two in-house standards. Additional samples were analyzed at the University of California, Riverside and University of Nevada, Las Vegas using a similar ThermoFinnigan GasBench setup.

Samples analyzed at the University of Michigan weighing a minimum of 10 μgrams were placed in stainless steel boats. Samples were roasted at 200°C in vacuo for one hour to remove volatile contaminants and water. Samples were then placed in individual borosilicate reaction vessels and reacted at 77° ± 1°C with 4 drops of anhydrous phosphoric acid for 8 minutes (a total of 12 minutes for dolomites, 17 minutes for apatite, and 22 minutes for siderites) in a ThermoFinnigan MAT Kiel IV preparation device coupled directly to the inlet of a ThermoFinnigan MAT 253 triple collector IRMS. O^{17} corrected data are corrected for acid fractionation and source mixing by calibration to a best-fit regression line defined by two NBS standards, NBS 18 and NBS 19. Data are reported in ‰ notation relative to VPDB. Precision and accuracy of data are monitored through daily analysis of a variety of powdered carbonate standards. At least four standards are reacted and analyzed daily. Measured precision is maintained at better than 0.5‰ for both carbon and oxygen isotope compositions.

5.4.4 Sulfur isotope analysis

Sulfur isotope analysis and elemental measurements were made at the University of California, Riverside. Samples were cut on a water cooled saw to remove weathered surfaces and any secondary carbonate phases including veins. Approximately 100 grams of each sample was crushed and powdered in a shatter box. 25-100 grams were then rinsed in DI water for 24 hours twice. The sample was then treated in a 4% hypochlorite (NaOCl) solution for 48 hours followed by two DI water rinses. The samples were then dissolved in 4 N HCl. The sample was centrifuged and vacuum filtered to remove the insoluble component. The dissolved SO_4 was reacted with saturated $BaCl_2$ solution ($\sim$ 250 g/L) to precipitate $BaSO_4$. The $BaSO_4$ was filtered, dried and weighed into silver capsules. The $BaSO_4$ was analyzed using an TC/EA coupled to a ThermoFinnigan MAT 253 IRMS. A 15 mL aliquot of the dissolved solution was measured on an ICP-MS for total SO_4 concentration.

5.5 Facies analysis, lithofacies associations and interpretation

5.5.1 Lithofacies association 1: Mid-ramp

crinkly laminite mudstone (Crl) The crinkly laminite mudstone is fine to medium laminated. The laminae have a tight crinkled texture (Fig. 5.3A). The irregular crinkled behavior of the laminae may indicate a microbial component to the sediment particularly because this laminite facies is the clasts composing the edgewise conglomerate rudstone facies suggesting a semi-consolidated seafloor (see below). This laminite can be disrupted during diagenesis and dewatering into a micro-nodular texture. This process is most common in beds that originally alternated between carbonate mudstone and pale yellow siltstone. Today the nodular carbonate floats within the fine siliciclastic matrix (Fig. 5.3E).

edgewise conglomerate rudstone (CrlEwc) The edgewise conglomerate rudstone is interbedded with the crinkly laminite mudstone facies. The beds are $\sim$ 5–10 cm thick and are composed of clasts of mudstone that are stacked on edge (Fig. 5.3B). These stacked clasts form rosette patterns on the bed tops (Fig. 5.3C). The mudstone clasts appear to have been only partially lithified during deposition as they are often compacted. This facies is interpreted as a rip-up deposit of the partially solidified surrounding sediment—crinkly laminite mudstone. An oscillatory wave action would stack clasts of the laminite on edge [48, 8].

These two lithofacies are found in both the Huqf Outcrop Area and the Oman Mountains and are interpreted as a mid-ramp lithofacies association. The sediments were likely deposited on a broad shallow shelf that was periodically swept by storms that generated the increased wave action required to create the edgewise conglomerate rudstone facies. These lithofacies have a $\sim$ 5 meter scale upward shallowing cycle where the edgewise conglomerate facies increases in abundance towards the top of the cycle (Fig. 5.20). This lithofacies association is only found in the Upper Shuram to Lower Buah Formation before the platform morphology changes from a gentle ramp to a rimmed shelf.

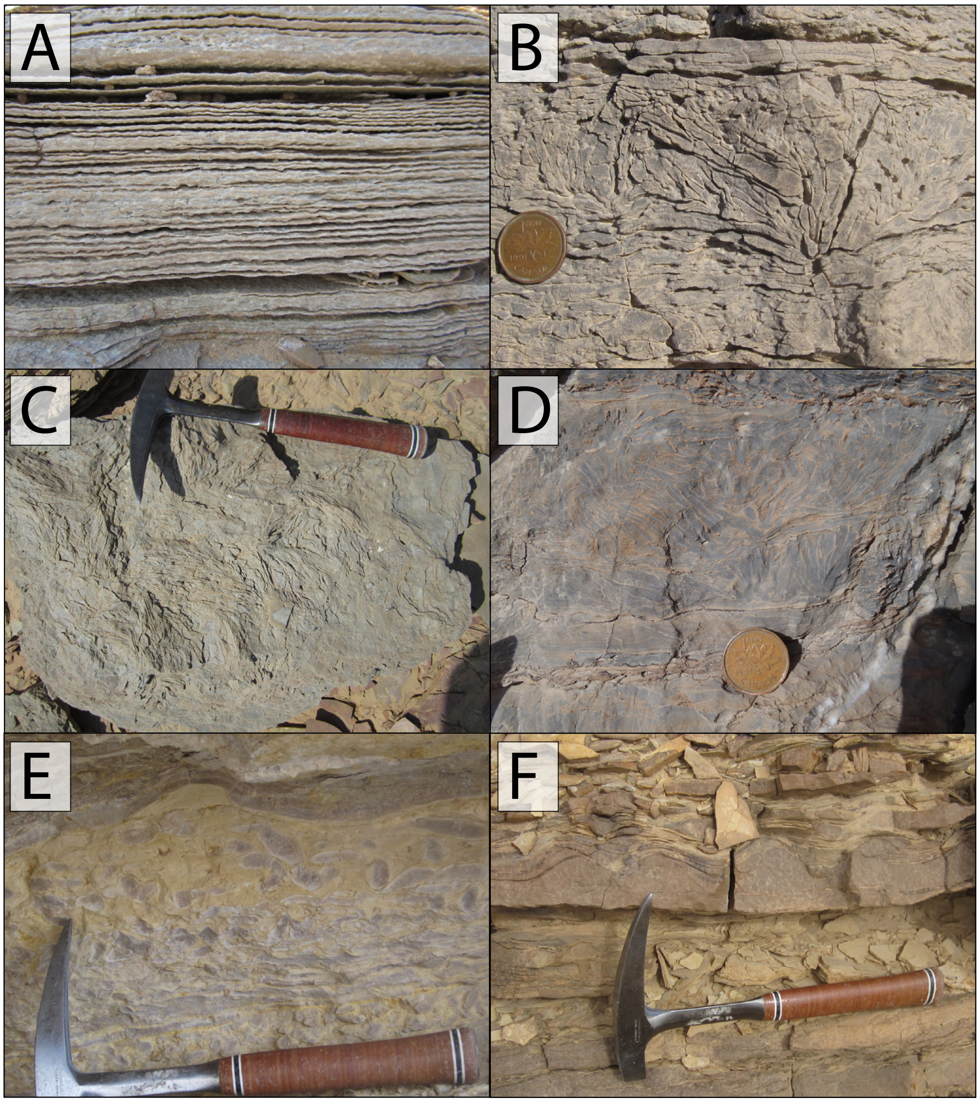

Figure 5.3: Representative lithofacies from LFA-1, the mid-ramp. A Crinkly laminite (Crl) B Edgewise conglomerates interbedded with crinkly laminite (CrlEwc). The edgewise conglomerate facies likely forms during storms when partially lithified crinkly laminite beds are reworked. C Bedtop of an edgewise conglomerate. D Edgewise conglomerate from the Oman Mountains with slightly thicker intraclasts. E Micro-nodular carbonate lenses in a pale yellow siltstone. F Rippled carbonate grainstone interbedded with pale yellow siltstones.

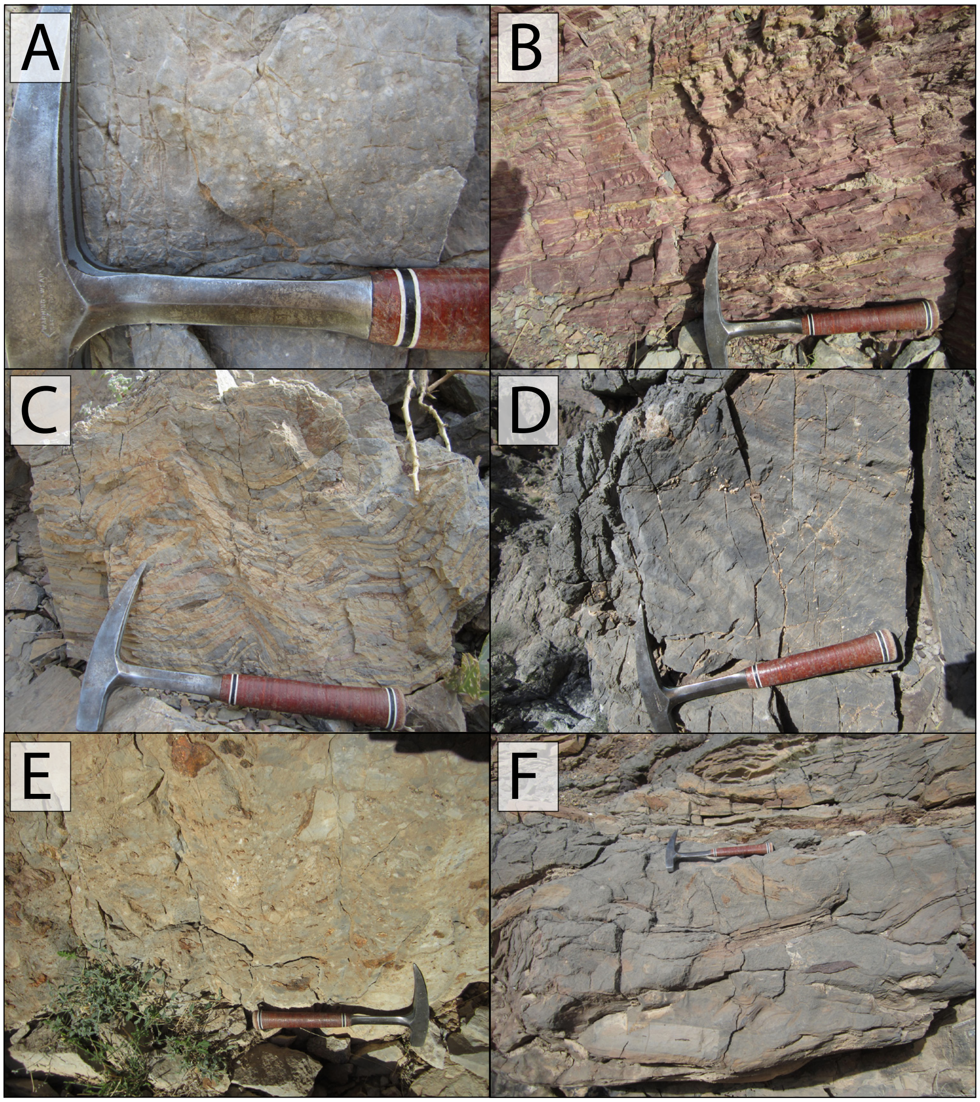

Figure 5.4: Representative lithofacies from LFA-2, the slope. A Giant ooid and mud chip event bed. B Deep red siltstones with carbonate lenses. C Disrupted and buckled carbonate wackestone interbedded with siltstones. D Brecciated thinly bedded packestone and very fine grainstone. The clasts are locally sourced and homogeneous. E Breccia with a variety of clasts including pale grey mudstones and oolitic grainstone. F Breccia with evidence for soft sediment deformation of some clasts.

5.5.2 Lithofacies association 2: Slope

matrix to clast supported rudstone (Brca) The matrix to clast supported rudstone has multiple variations that vary from bed to bed. In general the clasts are medium ($\sim$ 15 cm) to large ($\sim$ 50 cm). Some beds have clasts of mixed lithology including white mudstone, oolitic grainstone, and silicified clasts (Fig. 5.4E,F). Other beds are disrupted large clasts of the surrounding laminated mudstone to wackestone beds. Many clasts appear to be partially lithified and indicate later compaction (Fig. 5.4C,D).

siltstone (Sm) Siltstone intervals are interbedded with the matrix and clast supported rudstone facies. These siltstone are thin bedded and finely laminated. This facies is often red to tan in color in the Oman Mountains (Fig. 5.4B). This facies is most abundant in the Wadi Bani Awf section and increases in abundance in the lower Fara Formation.

planar bedded mudstone to wackestone (Ml/Wl). Planar bedded mudstone to wackestone beds are also interbedded with the matrix to clast supported rudstone facies. The wackestone beds can be more massive and include large ooids (Fig. 5.4A). In a few intervals the mudstone can be dark black in color and appears to have once been organic rich although no TOC measurements have been made.

These three lithofacies appear together in the Oman Mountains in the Upper Buah Formation and are interpreted as a slope lithofacies association. The sediments were likely deposited on the slope once the platform morphology transitioned to a rimmed shelf. The matrix to clast supported rudstone beds are interpreted as slope breccias that periodically punctuated the background sedimentation whether carbonate dominated mudstone or siltstone. These event beds vary from locally sourced breccias to further travelled breccia deposits that source a greater variety of sediment clasts. We interpret cored intervals in the subsurface well ZL-1 as analogous to this slope lithofacies association (Fig. 5.5). Similar matrix to clast supported rudstone facies are found throughout. There are even similar giant ooids to those found in the Wadi Bani Awf section in clasts of rudstone in ZL-1.

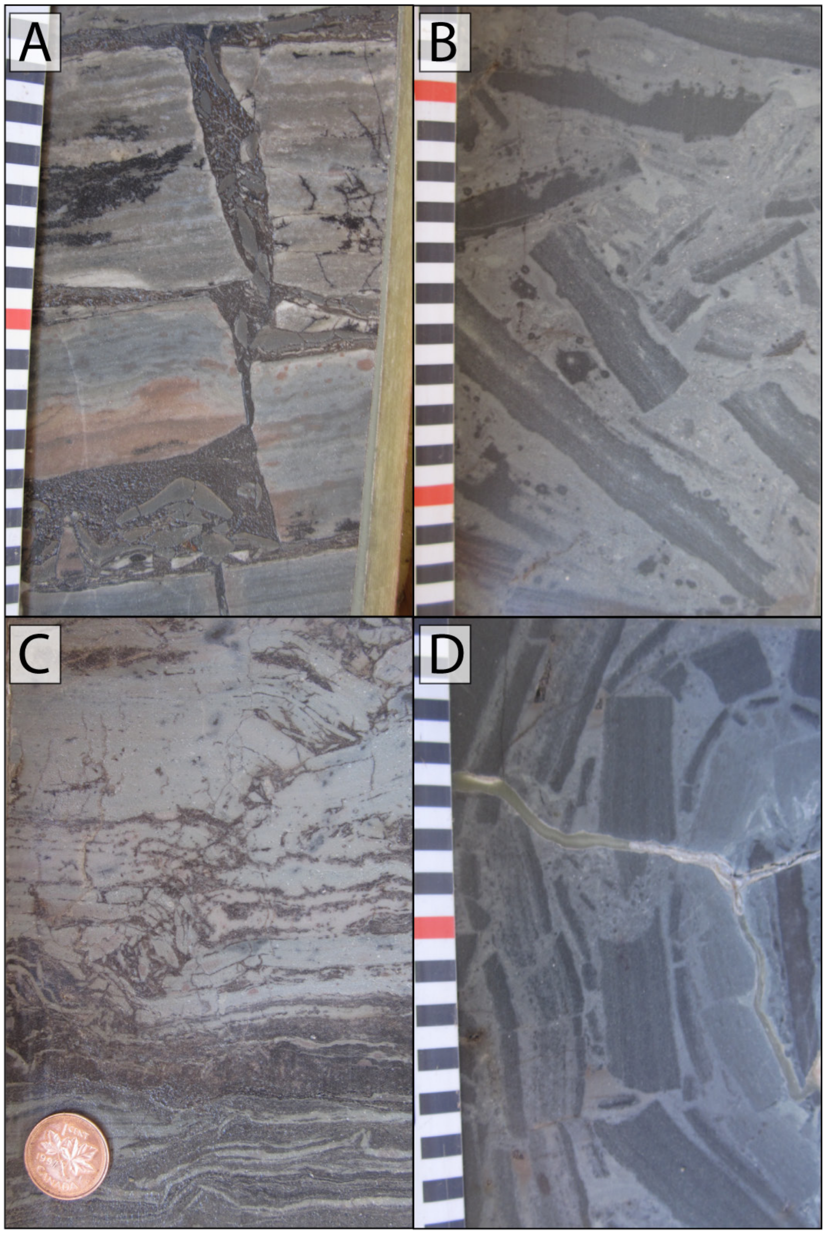

Figure 5.5: Representative lithofacies from well ZL-1. A-D Clast supported rudstone of barely moved mudstone to wackestone facies. These clasts can have recumbent folds (D) and indicate minimal lithification particularly of the bed tops (B).

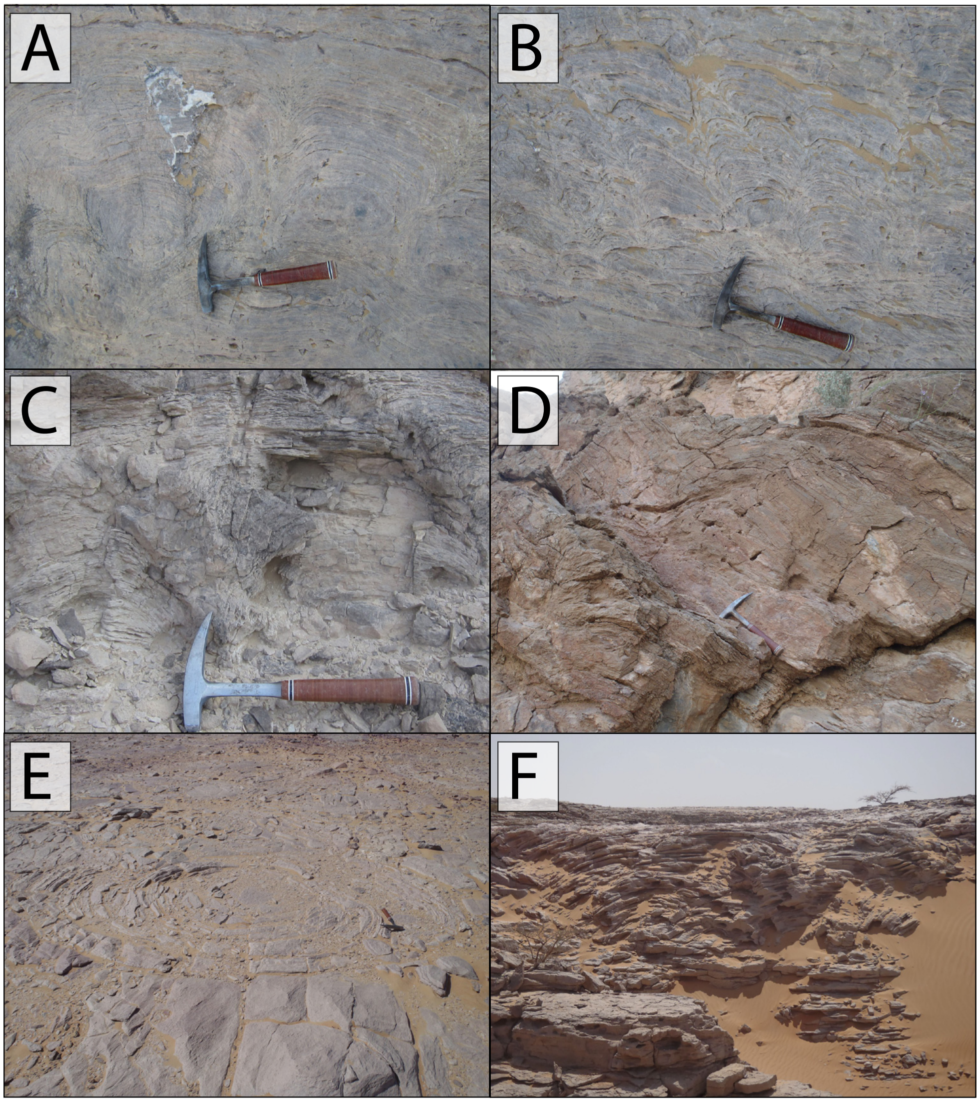

Figure 5.6: Representative lithofacies from LFA-3, the reef. A Medium stromatolites with coarse irregular laminae. B narrow stromatolites that form near the top of a parasequence. C Elongate medium stromatolites with coarse irregular laminae. D Large domal stromatolites from the Oman Mountains. E Bedding plane view of an elongate large domal stromatolite. F Overview of the stromatolite reef.

5.5.3 Lithofacies association 3: Reef

large domal stromatolite boundstone (Bldmstm) The large domal stromatolite boundstone facies is characterized by stromatolites over a meter in diameter that can grow and aggrade many meters in height (Fig. 5.6F). The laminae of these large stromatolites are irregular and of medium to coarse thickness. In multiple locations these stromatolites have significant spar-filled voids interpreted as primarily cavities in these large stromatolites that were filled with syn-sedimentary cements. In plan view these stromatolites can be elongate (Fig. 5.6E).
medium columnar stromatolite boundstone (Bmstm) Medium columnar stromatolite boundstone are closely associated with the large domal stromatolite facies (Fig. 5.6A). These smaller stromatolites have medium irregular laminae and can also be asymmetrically elongated (Fig. 5.6B). This facies can aggrade significantly while maintaining its columnar morphology.

These lithofacies appear in both the Huqf Outcrop Area and the Oman Mountains and are interpreted as a reefal lithofacies association. This lithofacies association overlies the mid-ramp lithofacies association and is interpreted to aggrade and prograde during a significant increase in accommodation, likely during flooding. We interpret the reef lithofacies association as the agent of change that causes the ramp morphology of the Khufai, Shuram and lowermost-Buah formations to evolve into a flat-topped platform morphology. The reef lithofacies association can be interbedded with the overlying shoal lithofacies association (described below) and has been termed the 'mound and channel' facies previously [8, 11]. Occasionally the medium columnar stromatolite boundstone facies is also found in the Wadi Hajir section in the Oman Mountains within the slope lithofacies association. In this instance the columnar stromatolites have much more narrow bases and then expand upwards and outwards. The laminae of these stromatolites are smoother.
thrombolite boundstone (Btbm) In the subsurface along the Eastern Flank of the South Oman Salt Basin and into the Northern Carbonate Domain, carbonates from the Birba Formation of the Ara Group have different dominant reef lithofacies. The Birba Formation reef lithofacies association is dominated by thrombolitic

boundstone that can vary in morphology significantly. Most are composed of mesoclots with occasional fine- scale morphology consistent with *Renalcis* growth habit. Other thrombolites can vary between more planar laminar morphologies and the opposite end-member a fingered vertical growth structure (Fig. 5.7). The stratigraphic isolation of stromatolites from thrombolites in the reef LFA suggests a potential community change that may have temporal significance.

Cloudina *grainstone (GCl)* Within the thrombolitic boundstone, a common co-occurring lithofacies is a *Cloudina* grainstone to packstone. These grainstone are dominantly composed of the early calcifying organism *Cloudina* and in core and thin-section calcified walls of the organism are visible (Fig. 5.7D)

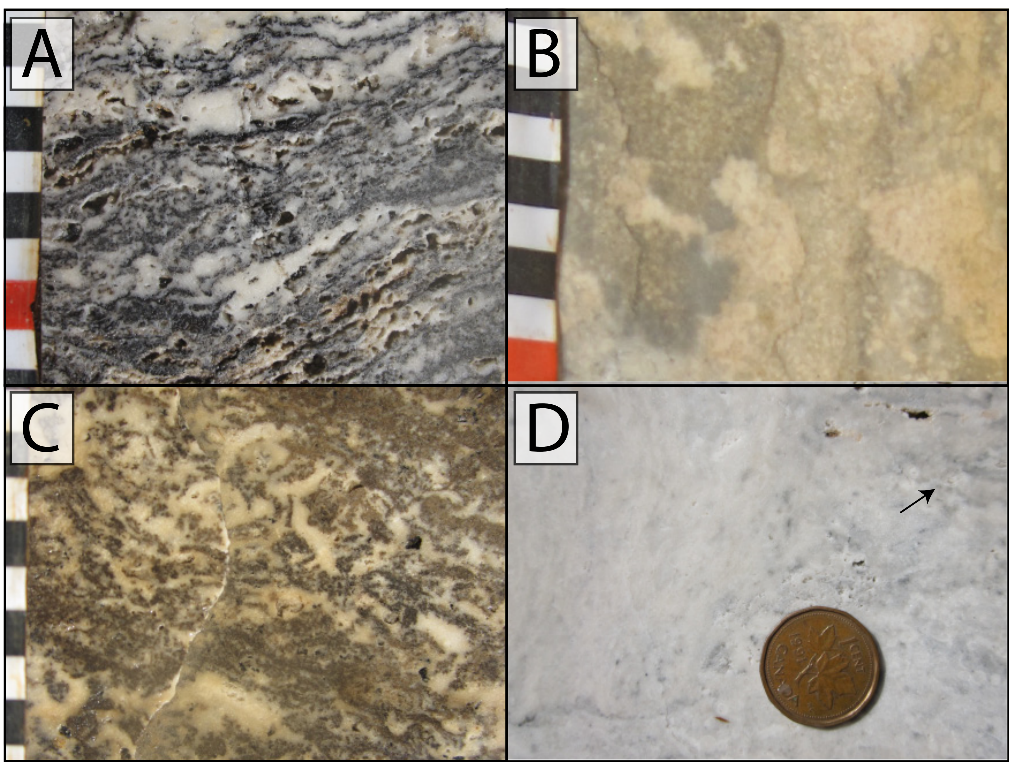

Figure 5.7: Representative lithofacies from LFA-3, the Birba-aged reef. A-C Thrombolite boundstone with mesoclots. D *Cloudina* grainstone filling in around a thrombolitic boundstone (left) (arrow pointing to example of *Cloudina*).

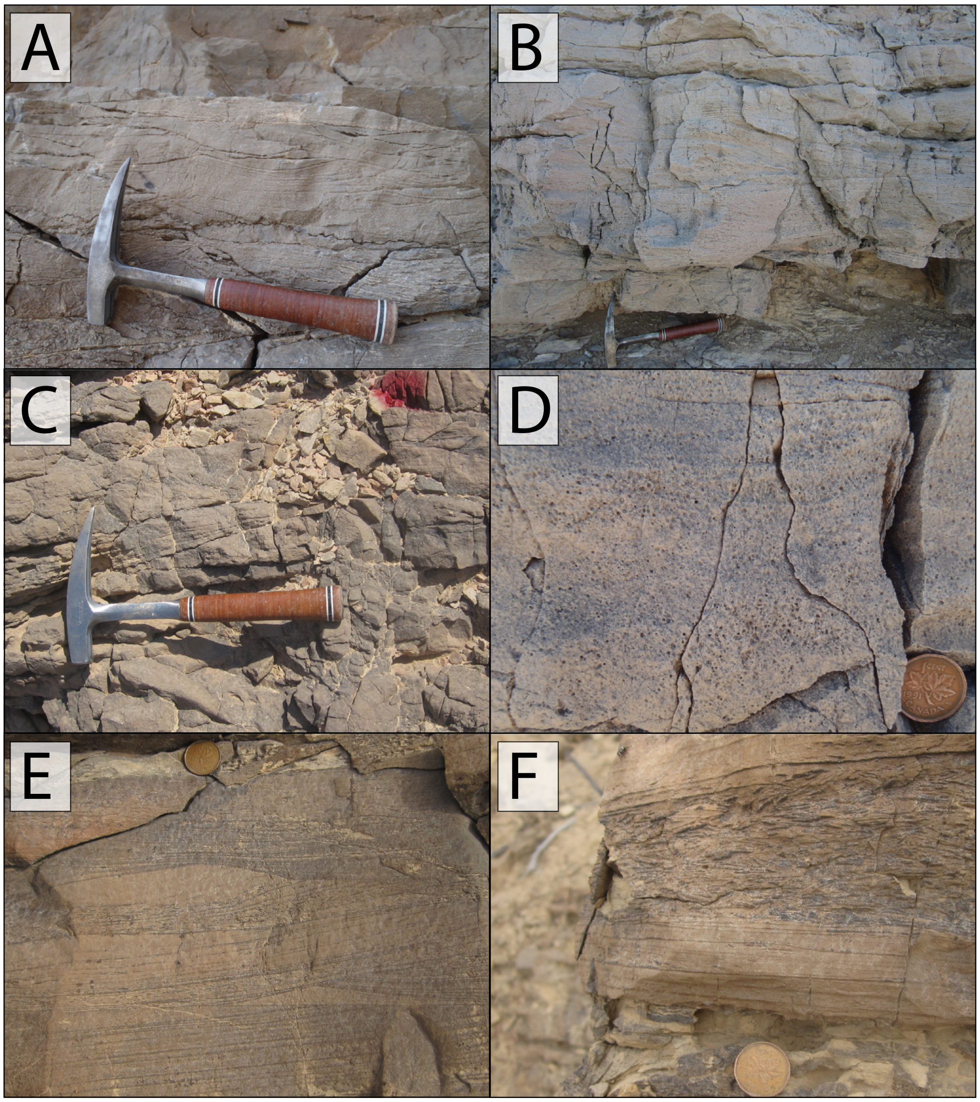

Figure 5.8: Representative lithofacies from LFA-4, the shoal. A Hummocky cross-stratified very fine grainstones. B Trough cross-stratified grainstone. C Trough cross stratified grainstone. D Oolitic grainstone. E Trough cross-stratified grainstone and chip breccia. F Close-up of a chip breccia bed.

5.5.4 Lithofacies association 4: Shoal

swaley to hummocky cross-stratified grainstone (Ghcs) The swaley to hummocky cross-stratified grainstone facies is typified by low angle truncations and gentle hummocks (Fig. 5.8A). Bedding is $\sim$ 10's of cm. The grainstone is very fine grained and composed of peloids.

trough cross-stratified grainstone (Gt) The trough cross-stratified grainstone has higher angle truncations (Fig. 5.8B,C). In some beds the grains are small intraclast mudchips as well as very fine peloids (Fig. 5.8E,F).

oolitic grainstone (Goo) The oolitic grainstone can have sedimentary structures including trough and swaley cross-stratification (Fig. 5.8D). The ooids are usually fine to medium grained and the laminar concentric structure is often largely obscured by micritization while the cores have been dissolved and replaced with blocky cement (Fig. 5.16D).

These lithofacies occur in both the Huqf Outcrop Area and the Oman Mountains and are interpreted as a shoal lithofacies association. This lithofacies association interfingers with and overlies the reef lithofacies association. Oolitic grainstone facies are common in the Oman Mountains and near the top of the Shoal lithofacies association however the coarser grainstone have a higher tendency for recrystallization in the shoal lithofacies association likely because of high primary porosities which can lead to fabric-destructive diagenesis.

Previous researchers have interpreted the boundary between the shoal and first occurrence of lagoonal lithofacies associations as a major hiatus and sequence boundary—naming this the formation boundary between the Buah and proposed Sirab formations [11, 15, 10, 5, 4].

5.5.5 Lithofacies association 5: Lagoon

evaporitic siltstone to silty mudstone (Sm) The evaporitic siltstone deposits are often deep red or pale green and can be poorly lithified in outcrop. The silty mudstone can have features indicative of restriction including evaporite laths and

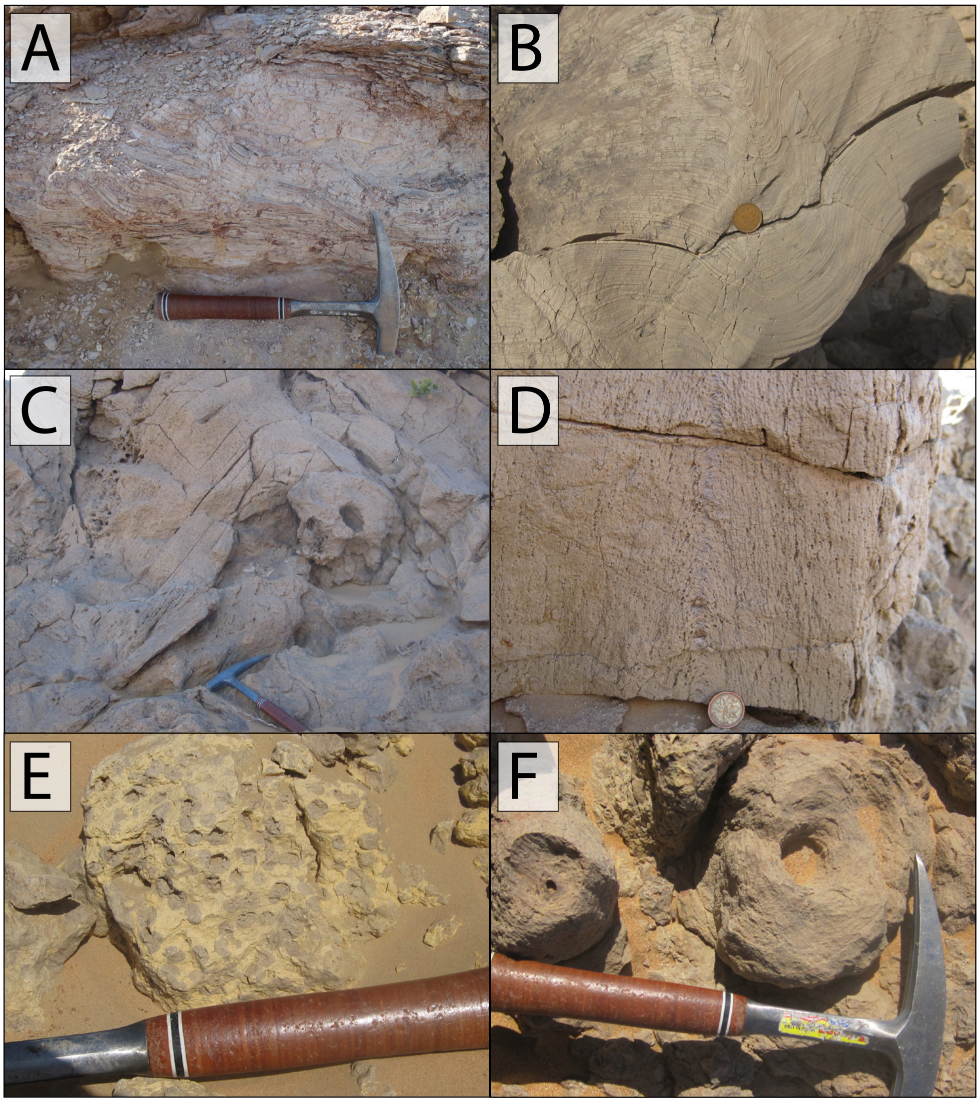

Figure 5.9: Representative lithofacies from LFA-5, the lagoon or subtidal backshoal. The low-energy facies that develop during in the Sirab Formation on the platform top include silt-rich carbonate mudstones and some stromatolite facies. Notably during the maximum flooding interval above SB-2, a platform top buildup of *Conophyton* stromatolites occurs. A very thinly bedded carbonate mud-rich siltstone. B Isopachochous stromatolite with a strong precipitation component. C Large *Conophyton* stromatolite. D The axial plane of a *Conophyton* stromatolite. E Spheroidal weathering texture common in the *Conophyton* build-up. F Two smaller *Conophyton* stromatolites.

gypsum rosettes as well as fenestrae and mudcracks. The silt-rich facies tend to be poorly exposed and are often covered intervals in most sections but are better exposed in sections MD1 and MD2.

irregularly laminated stromatolite boundstone (Bilstm) The irregularly laminated stromatolites are characterized by highly irregular often heavily silicified laminae. The morphology varies from columnar in morphology to more conical. Some of these stromatolites have evaporite pseudomorphs encrusting them and within individual laminae.

isopachous stromatolite boundstone (Bisstm) These stromatolites are characterized by very even laminae that often display chevron style junctions with between neighboring stromatolites (Fig. 5.9B). The laminae do not thicken and thin significantly along the sides of the stromatolite and often accommodate very steep angles of repose [49, 50]. In thin section and in hand sample these stromatolite laminae are dominated by precipitation although the individual crystal blades are not always preserved. They lack sediments between the stromatolites.

conophyton stromatolite boundstone (Bconstm) The *Conophyton* stromatolites are conical in morphology and look like missiles in outcrop (Fig. 5.9C,D,F). Individual *Conophyton* vary in height ($<$ 2 meters), width and the morphology. The size of individual *Conophyton* stromatolites scales with available accommodation space (see ST1, ST2, ST3, WS3). In some stromatolites the characteristic axial plane can be found that relate these Ediacaran *Conophyton* stromatolites to Mesoproterozoic *Conophyton* stromatolites (i.e., Dismal Lakes Group, Canada and the Afar Group, Mauritania) [51, 52]. The lamination style of these stromatolites is unique and consists of medium laminae that in thin section are composed of intergrown spherulitic precipitates (Fig. 5.16A). These spherulites have a cloudy center and faint radial morphologies. The cavities between the spherulitic laminae are infilled with clear sparry calcite cements. The matrix of the *Conophyton* stromatolites is mud rich and contains abundant spheroidal structures likely microfossils with a simple wall (Fig. 5.16F). Near the base of the *Conophyton* stromatolites in almost all outcrop exposures, an interesting diagenetic feature of larger pale yellow spheres cross-cuts laminae (Fig. 5.16E).

We interpret all of these lithofacies to form in a low-energy lagoonal depositional environment on the platform top in a wide range of water depths from very shallow to deeper. The lagoonal lithofacies association repeats three times within the stratigraphy of the Huqf Outcrop Area. The first lagoonal deposits overlay the shoal lithofacies association. These lagoonal deposits are shallow to very shallow and restricted with abundant evaporite pseudomorphs, gypsum rosettes and chicken wire nodules. These deposits contain cycles ($\sim$ 2–6 meters thick) that begin with siltstone at the base and grade into carbonates (Fig. 5.20). The capping carbonates include small columnar stromatolites with evaporite pseudomorphs within the laminae and silicification as well as tepee structures. Some of the beds within these lagoonal deposits are laterally traceable across the entire Huqf outcrop area indicating a very at-topped platform The second repetition of lagoonal deposits overlay carbonates from the peritidal carbonate lithofacies association and are similarly restricted to the first. The carbonate beds capping the siltstones are very silicified and composed of irregular to columnar stromatolites. The third repetition of lagoonal deposits begins much deeper than the first two lagoon deposits. A significant increase in accommodation space—likely during a transgression—allows patch reefs of *Conophyton* and isopachous stromatolites to form within the lagoon on the platform top. These reefs are overlain by grainstone deposits and more restricted lagoonal deposited dominated by red siltstones interbedded with thin beds of columnar to isopachous stromatolites.

5.5.6 Lithofacies association 6: Peritidal

intraclast conglomerate rudstone (Icg) The intraclast conglomerate rudstone facies is characterized by massive mudstone chip intraclasts within a mudstone matrix. This facies also often has coarse sand grains within the matrix (Fig. 5.10F). The beds are usually thin ($\sim$ 5–10 cm).

massive mudstone (M, Mf, Mfal, Mal, Wgp) The massive mudstone is usually light grey and often contains features including fenestrae, evaporite laths

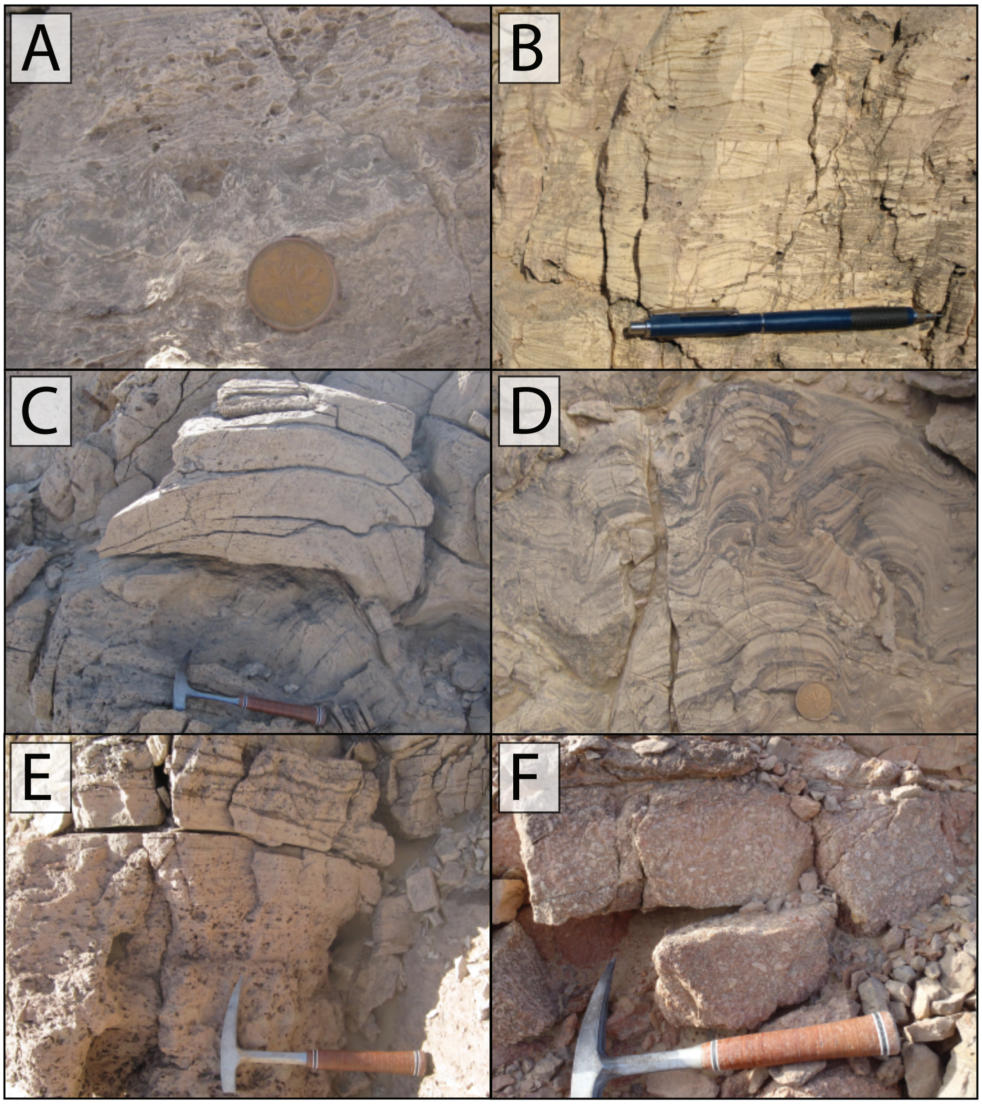

Figure 5.10: Representative lithofacies from LFA-6, the intertidal zone. A Tufted laminite. B Rippled grainstone often with climbing ripples indicating significant aggradation during deposition. C Elongate domal stromatolites. D Smaller narrow stromatolites with more of a siliciclastic component. E Fenestral mudstone often with spar-filled fenestrae and anhydrite laths or gypsum rosettes. F Intraclast conglomerate with a significant quartz sand component.

and occasionally larger gypsum pseudomorphs. The massive mudstone beds are thin (~ 5–10 cm) and when an intraclast conglomerate rudstone is present the mudstone is found overlying it.

domal stromatolite boundstone (Bdmstm) The low domal stromatolite boundstone are generally a half a meter to a meter in width. They can aggrade over a meter in high but do not indicate significant synoptic relief. The domal stromatolite laminae are thick and are almost always fenestral (Fig. 5.10C,E). The fenestrae are round to oblong and can be spar filled or open (Fig. 5.16C). These domal stromatolites are almost always very elongate forming parallel rows of domal stromatolites in plan view indicating they formed in the presence of a current likely tidal currents (Fig. 5.10C).

small columnar stromatolite boundstone (Bsmstm) The small columnar stromatolite boundstone have interconnected laminae between individual stromatolites. The laminae are generally smooth however the thickness of the laminae vary from the sides of the stromatolites to the troughs between them. These stromatolites often show minor asymmetrical elongation likely from current activity. In thin section these stromatolites are composed of mud to very fine-grained peloids (Fig. 5.10D).

rippled grainstone (Grip) The rippled grainstone facies is composed of fine peloidal grains and occasionally fine ooids. The rippled grainstone indicates aggradation during deposition and often preserve asymmetrical climbing wave ripples (Fig. 5.10B). Bedding plane surfaces preserve ripple crests.

irregular to tufted laminite boundstone (Bil) The irregular to tufted laminite boundstone is characterized by fine irregular laminae with small upward tufts (Fig. 5.10A). The laminae can be more irregular and are often heavily silicified. In general this microbial boundstone facies is characterized by low relief.

sandstone (Ss) The sandstone facies is medium to coarse grained and is quartzose-feldspathic. Sandstone beds are massive and vary in thickness from 1–5 meters. While sandstone facies are not common in this platform margin, there is a persistent sandstone marker bed, previously designated as the boundary between the

Lower and Upper Shital Members [4, 5]. We interpret this as a transgressive sandstone that sits at a sequence boundary (SB3) between shallow lagoonal facies and peritidal facies.

These facies are interpreted to form in the peritidal environment with water depths ranging from the shallowest subtidal environment through the intertidal zone. We have arranged individual facies within this facies association in approximate position within a given shallowing upward cycle although not every facies is present in each cycle (i.e., sandstone). In general the shallowing upwards cycle that characterizes the peritidal facies association is an occasional base of intraclast conglomerate, interpreted as a transgressive lag deposit, a massive mudstone that grades into fenestral low domal stromatolites. These are capped by small columnar stromatolites, rippled grainstone and finally irregular laminite. The facies from subsurface cores from well SWT8 are similar and include columnar stromatolites interbedded with wackestone with the occasional mudstone drape and ooid grainstone and intraclast conglomerate (Fig. 5.11). In the cores from SWT8, there is an increased component of seafloor precipitation within some stromatolites and sediments (Fig. 5.11A,D,E). We interpret these facies in the subsurface as analogous to the outcrop peritidal lithofacies association.

5.5.7 Lithofacies association 7: Supratidal

irregular to pustular laminite (Bil) The irregular to pustular laminite is characterized by more bulbous and pustular morphology (Fig. 5.12C). This facies has significant primary porosity remaining indicating cementation by vadose processes were not significant enough to occlude the porosity built into the primary growth morphology. Some irregular laminite have gypsum pseudomorphs within them. Petrographically, they can preserve the rhombohedral walls and classic twinning (Fig. 5.16B,G).

tepee pisolite (Tep, Pis) The tepee-pisolite facies is characterized by abundant tepee structures and a variety of pisolite morphologies and is broadly similar to other documented tepee-pisolite occurrences [53, 54, 55, 56]. This facies

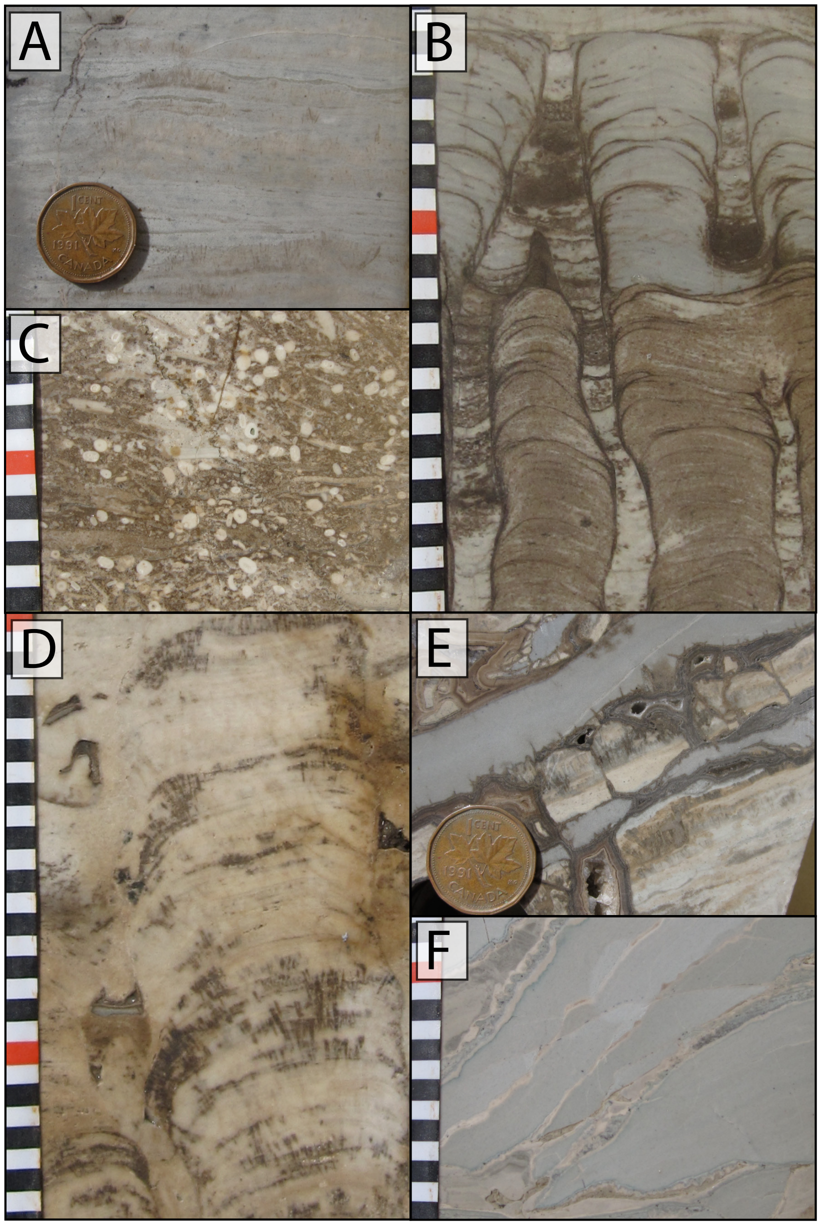

Figure 5.11: Representative lithofacies from well SWT-8. A Fine wackestone beds with occasional mud drapes. Some of the wackestone beds have precipitated crystal fans growing in them in what appear to be more massive potentially microbial regions of the beds. B Tall columnar stromatolites that display a small amount of elongation in cross section. The inter-stromatolite fill has some larger peloidal grains. C Giant ooid and mud chip intraclast packstone. D Columnar stromatolite that is more dominated by precipitated crystal fans in a more massive matrix with some primary voids with geopetal mudstone fill. E Mudstone and wackestone beds with abundant crystal fan precipitates that were then brecciated and cemented with multiple generations of isopachous cement and geopetal mudstone. F Brecciated and cemented wackestone with isopachous cements and geopetal mudstone filling between the primary beds.

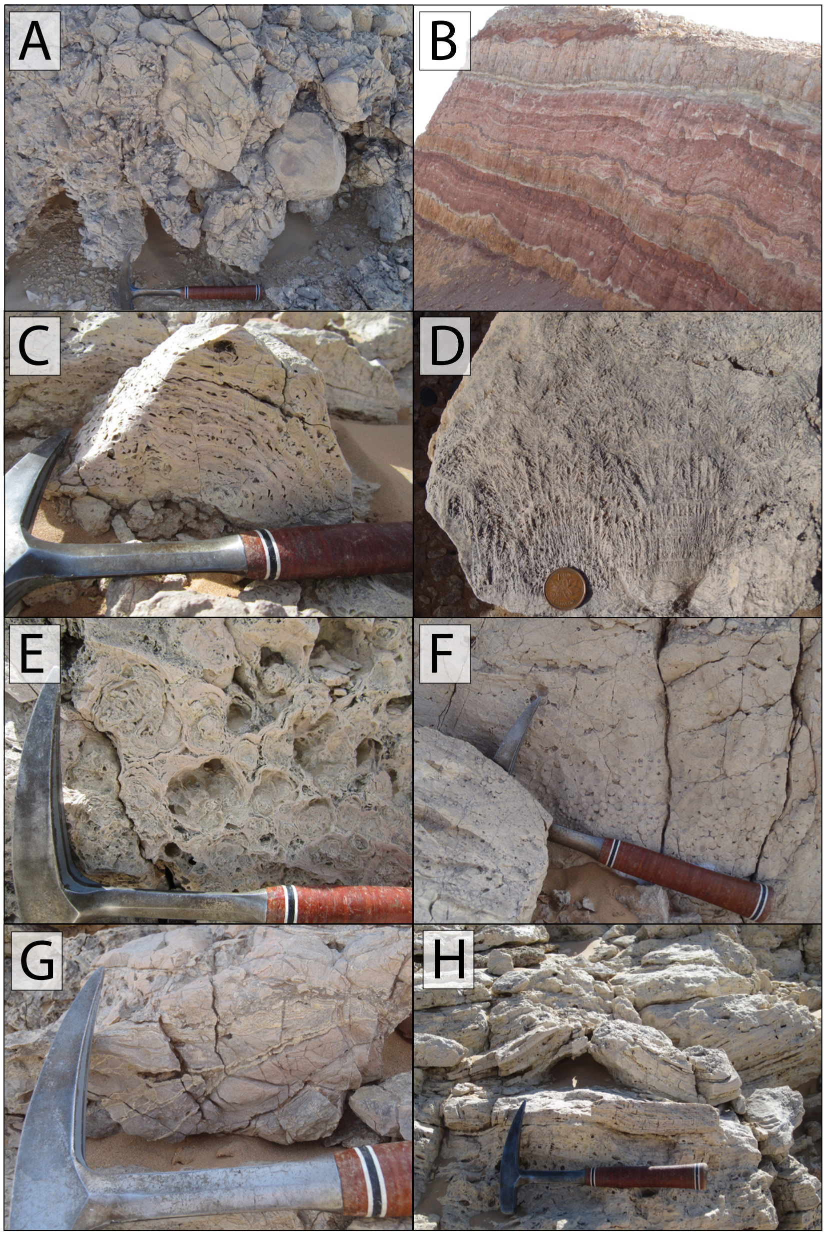

Figure 5.12: Representative lithofacies of LFA-7, restricted environments from the uppermost Sirab Formation. A Karst breccia from SB-3. B Red siltstones alternating with carbonate mudstones from SB-3. C Irregular laminite. D Tufa from SB-3. E Large pisoids. F Very round precipitation dominated pisoids. G tepeed and cemented mudstone. H tepeed irregular laminite.

alternating with the irregular to pustular laminite facies is quite thick in one area of the Huqf Outcrop Area ($\sim$ 150m). Within this thick deposit the pisoids vary from precipitation dominated pisoids with thick rinds of bladed cement (Fig. 5.12F), to pisoids that can grow quite large ($\sim$ 10 cm) of fine micritic irregular laminae (Fig. 5.12E). Petrographically, multiple generations of cement coating the micritic pisoid cores can be identified including radial isopachous cement (Fig. 5.16I,H) and clear porosity-occluding cement (Fig. 5.16H). These pisoids fill in between tepee structures of all sizes from multiple meters tall to quite small (Fig. 5.12G,H). Similar to the pisoids, some tepee structures have significant floor and pendant bladed cements as well as geopetal mudstone (Fig. 5.12G) while other tepee structures maintain their original high primary porosity Fig. 5.12H). Occasional silica cementation of small round nuclei occurs (Fig. 5.16E).

tufa (Tfa) A marker bed (sometimes karsted) can be found across the Huqf Outcrop Area of a tufa characterized by interconnected branching carbonate precipitates (Fig. 5.12D). The tufa likely formed from a supersaturated brine associated with extreme exposure of the platform associated with SB4 [49, 50].

paleokarst breccia (Brca) A paleokarst surface with variable degrees of brecciation is found in the Huqf Area underlying the thick tepee-pisolite facies. The breccia often form pipes into underlying stratigraphy and can include blocks of the tufa facies. In general the matrix is carbonate cemented and the brecciation generally preserves the prior stratigraphy.

salt collapse breccia (Brca) A series of outcrops previously undocumented near Bantawt preserve a sequence of sediments including evaporite-rich, brecciated mudstone and siltstone. These are capped by a heavily silicified breccia that can preserve very large blocks (Fig. 5.13A) with inclined near-vertical bedding. The blocks preserved within this breccia are mixed lithology and do not obviously source local facies. Blocks include irregular laminite (Fig. 5.13B).

These facies are interpreted to form in a dominantly supratidal environment that is periodically subjected to rewetting [53, 54, 55, 56]. There are short ($\sim$ 1 meter) cycles of irregular to pustular laminite that grade into tepee structures

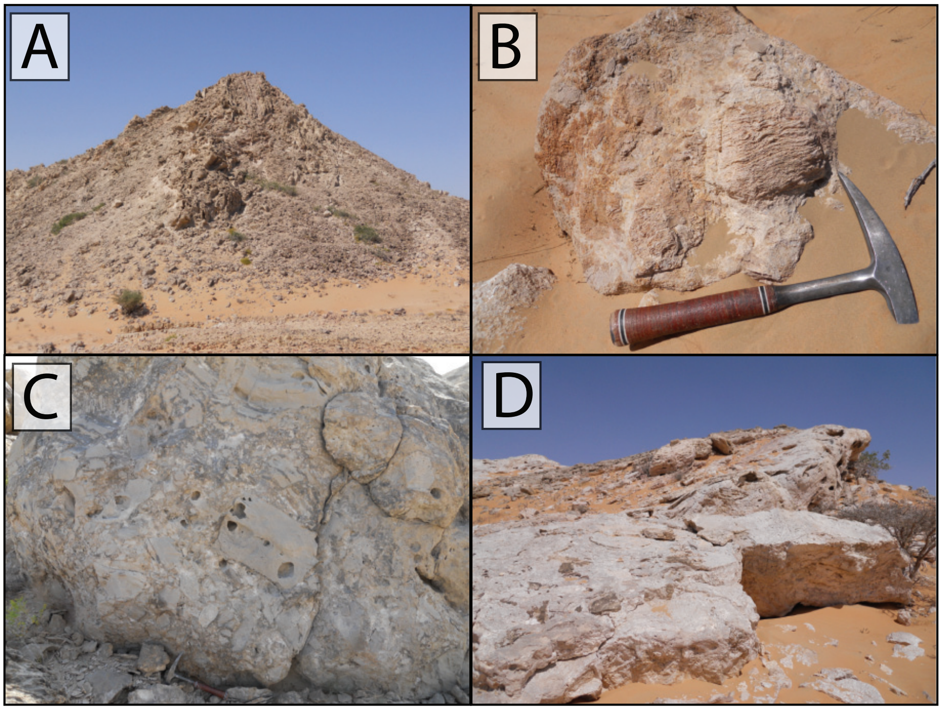

Figure 5.13: A different outrcrop area of LFA-7. A large block with steeply inclined bedding. B Breccia with clasts of irregular laminite. C Silicified breccia with very large clasts. D tepeed and spar dissected mudstone.

and pisoids. The subsurface cores from nearby SWN1 have very similar lithofacies including irregular laminite, tepee structures with floor and pendant cements and pisoids (Fig. 5.14). The wells on the Eastern Flank also have similar facies preserved in cored intervals including karst breccia, tepee structures, pustular laminite and pisoids (Fig. 5.15). We also interpret these subsurface lithofacies as belonging to the supratidal lithofacies association.

5.6 Sequence stratigraphy

Three levels of cyclicity were identified within the stratigraphy of the Huqf Outcrop Area. Within each lithofacies association meter-scale cyclicity, termed here 'parasequence', were identified. These parasequences are cycles with a transgressive (flooding) and regressive (shallowing) component [57, 58]. Schematic parasequences from each lithofacies association (Fig. 5.20) indicate most of the cycle is

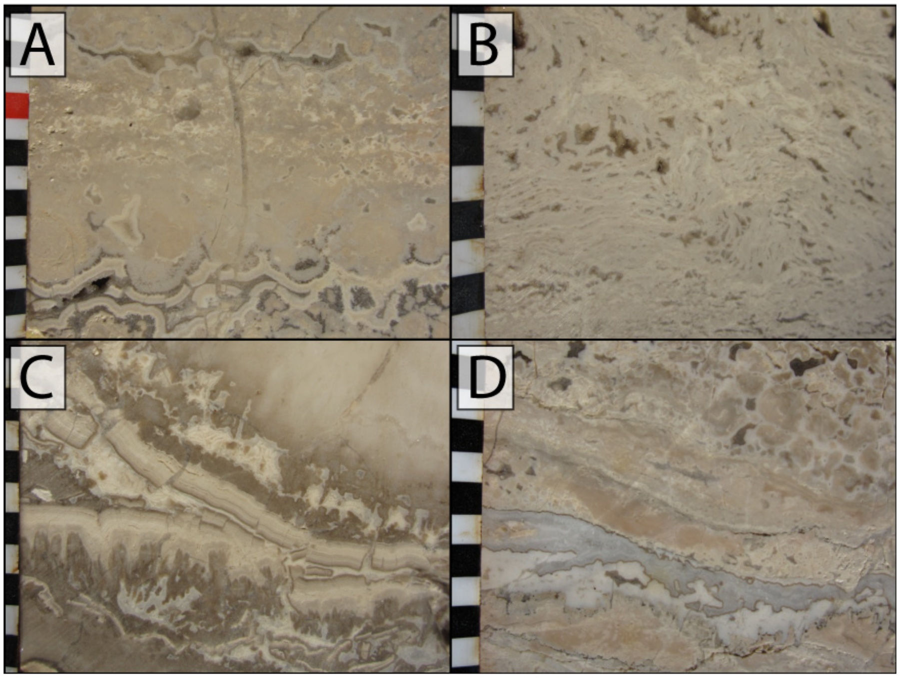

Figure 5.14: Representative lithofacies from well SWN-1. A Pisoids with multiple generations of isopachous cement. B Irregular to tufted laminite. C tepeed mudstone with fibrous pendant and floor cements filled in with geopetal mudstone. D tepeed mudstone with fibrous cements filled in with geopetal mudstone capped by pisoids.

regressive with a small component of transgression particularly within the peritidal and supratidal sequences.

The second level of cyclicity, termed here the 'parasequence set', is generally 10-15 meters in thickness and composed of multiple successive parasequences. The parasequence set also has a regressive and transgressive component and towards the top of a given parasequence set the relative proportion of deposition in the regressive portion of the parasequences increases.

The third level of cyclicity, termed here the 'sequence', is on order 50-100 meters in thickness. The sequences contain multiple lithofacies associations stacked on top of one another and also have a transgressive and regressive component. The transgressive component of the sequence is characterized by retrogradation and a general landward shift of the shoreline whereas the regressive component is dominated by aggradation and progradation and an oceanward shift in the shoreline [57, 58]. This level of cyclicity is most easily identified in the shallow water

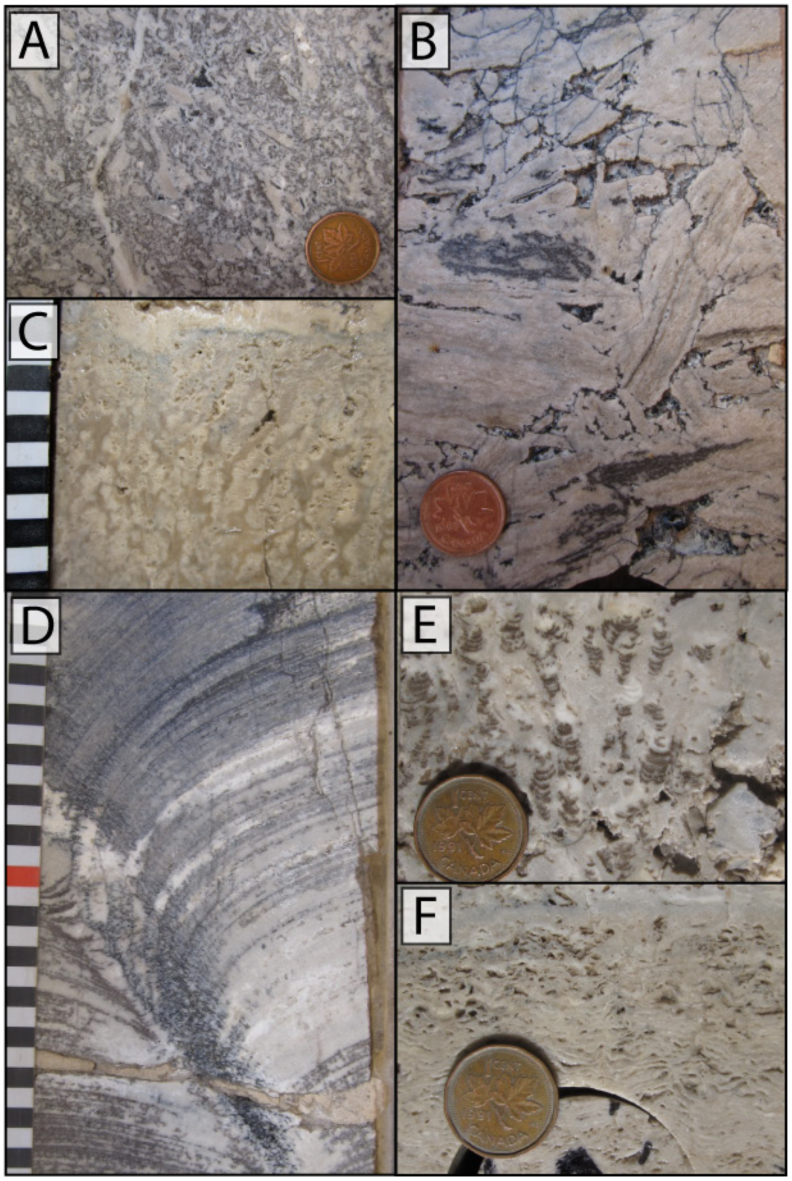

Figure 5.15: Representative lithofacies from subsurface wells along the Eastern Flank. A irregular microbial boundstone with brecciation and cement pockets. B In situ brecciation associated with exposure and karst. C upward growing pustular microbial dendrites. D precipitation dominated isopachous stromatolite. E unusual microbial structure similar to a tufted laminite with more regular concave laminae between the tufts. F tufted laminite with some remaining porosity.

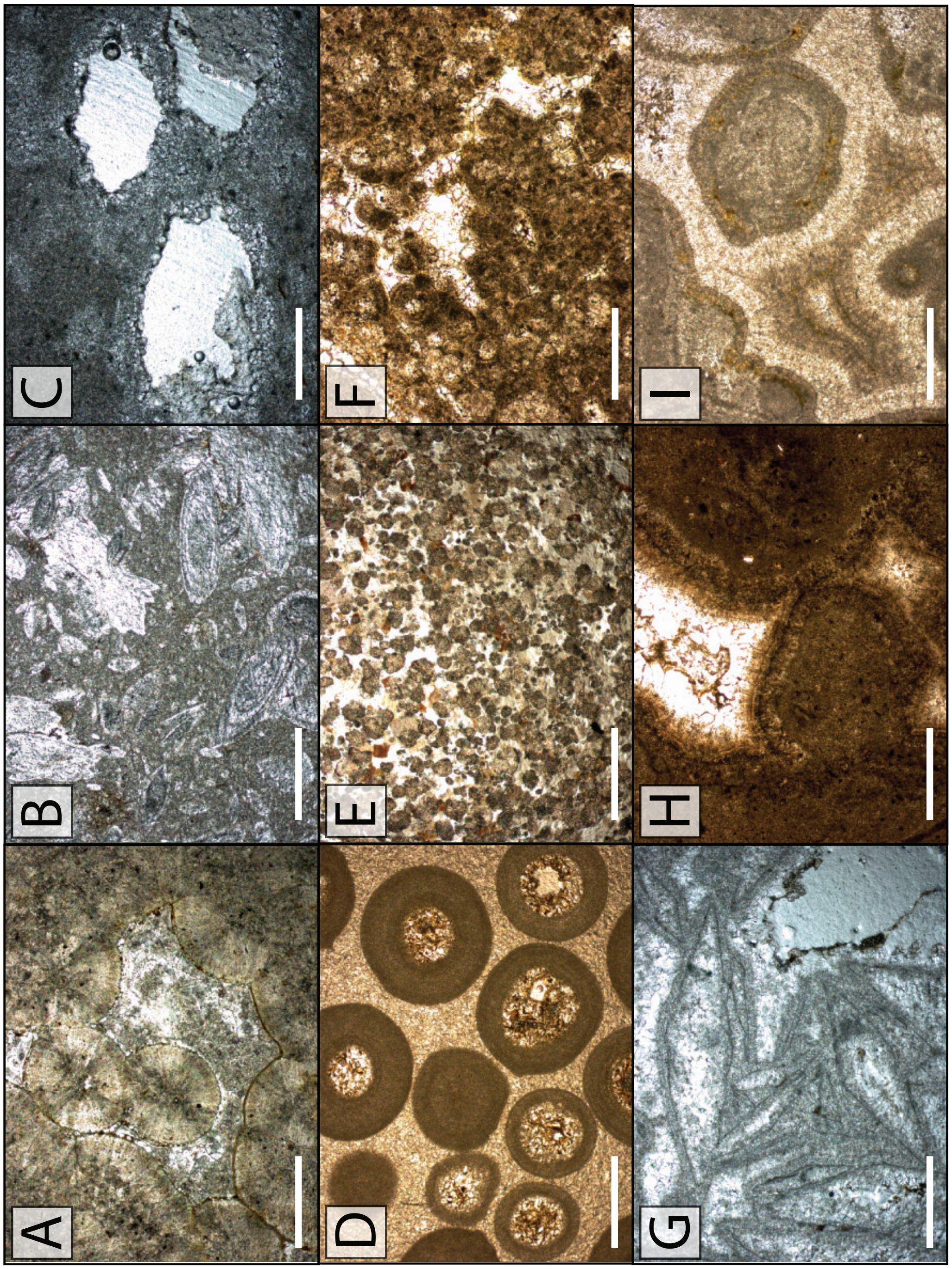

Figure 5.16: Thin section photomicrographs of key lithofacies from the Huqf. A *conophyton* spherulite texture showing organic matter in the center of the spherulites. B Gypsum crystals showing characteristic twinning. C Fenestral mudstone with open oblong fenestrae partially filled with micritic mudstone. D oolitic grainstone with micritized outer laminae and dissolved interiors replaced with blocky cements. E silica cemented microspheroids of calcite. F mudstone matrix surrounding the *conophyton* stromatolites with possible thin-walled microfossils. G rims of gypsum crystal rhombs. H Irregular laminae of a pisoid cemented with fibrous isopachous cement and clear blocky cement. I Pisoids with thick isopachous fibrous cements coating the original grains and occluding porosity.

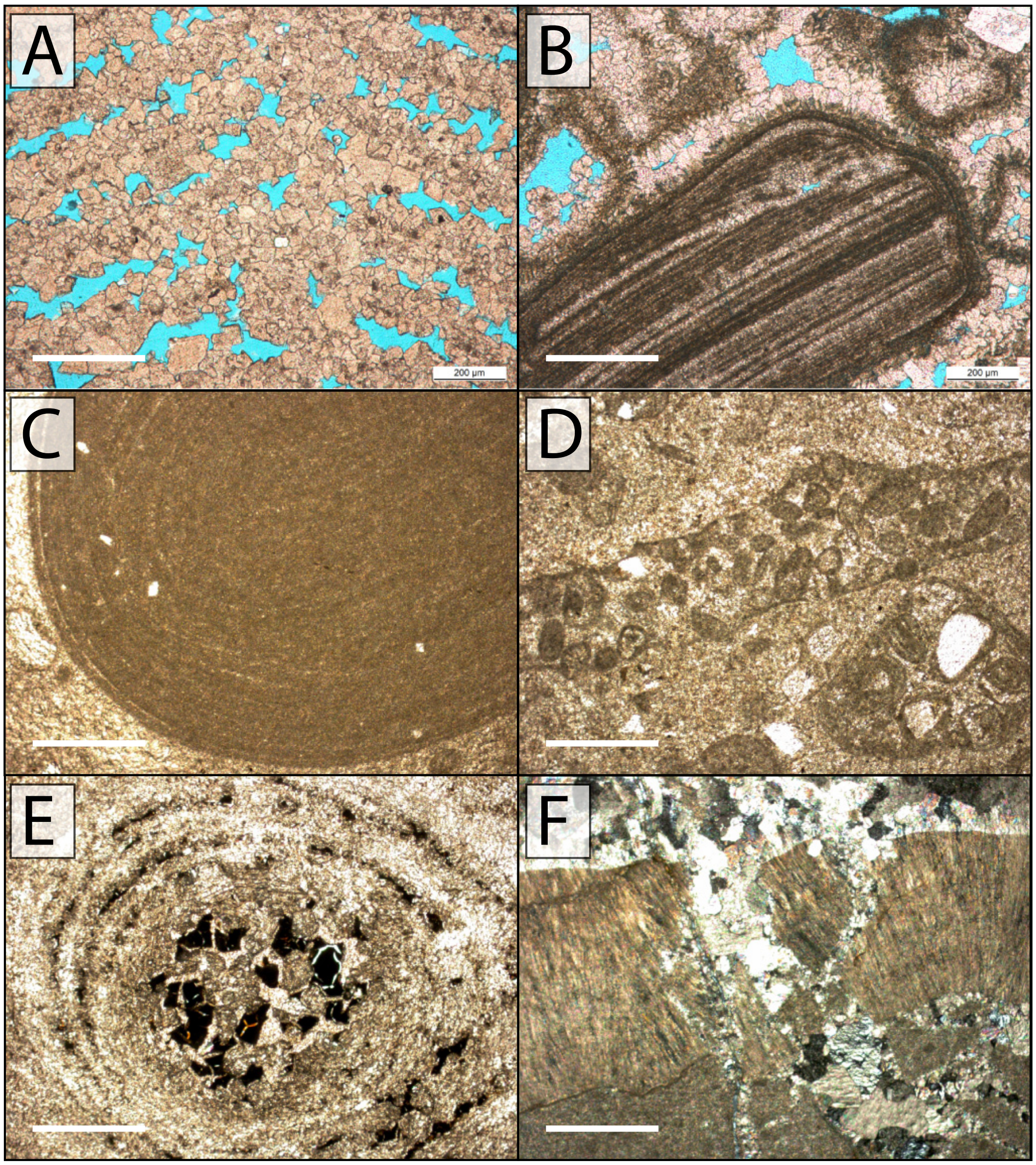

Figure 5.17: Thin section photomicrographs of key lithofacies from the subsurface. A Dolomitized tufted laminite with preserved primary porosity between laminae. B Intraclasts including a laminated clast coated with early cements before being dolomitized. C Giant ooid with micritization of the original laminae. D compound intraclasts composed of dominantly peloids and ooids. E concentric walls of *Cloudina*. F Brecciation within a tepee structure with isopachous fibrous cement.

BOUNDSTONES			
	Bldmst m	large domal stromatolite, can be elongate	LFA 3: Reef
	Bmstm	medium stromatolite	LFA 3: Reef
	Bdmst m	domal stromatolite, can be elongate, laminae can be fenestral and spar-filled	LFA 6: Peritidal
	Bsmst m	small stromatolite, laminae usually smooth	LFA 6: Peritidal
	Bconst m	conophyton stromatolite, composed of spherulites, form bioherms, organic-rich	LFA 5: Lagoon
	Bisstm	isopachous stromatolite, fine smooth even laminae	LFA 5: Lagoon
	Becstm	egg carton stromatolite forms at SB3, white micritic laminae	LFA 7: Supratidal/ Restricted
	Bilstm	irregularly laminated stromatolite	LFA 7: Supratidal/ Restricted
	Bil	irregular to tufted laminite	LFA 7: Supratidal/ Restricted

MUDSTONES and WACKESTONES			
	Crl	crinkly laminite	LFA 1: Mid-Ramp
	CrlEwc	crinkly laminite and edgewise conglomerate	LFA 1: Mid-Ramp
	Ml/Wl	laminated mudstone/wackestone	LFA 2: Slope & LFA 6: Peritidal
	Mf	fenestral mudstone	LFA 6: Peritidal
	Mfal	fenestral mudstone with anhydrite laths	LFA 6: Peritidal
	Mal	mudstone with anhydrite laths	LFA 6: Peritidal
	Wgp	wackestone with gypsum pseudomorphs	LFA 6: Peritidal

Figure 5.18: Boundstone, mudstone and wackestone lithofacies key

PACKSTONES and GRAINSTONES			
	Gt	trough cross stratified grainstone	LFA 3: Shoal
	Goo	oolitic grainstone	LFA 2: Slope & LFA 3: Shoal & LFA 6: Peritidal
	Gma	massive grainstone	
	Ghcs	hummocky cross stratified grainstone	
	Grip	rippled grainstone (often climbing)	LFA 6: Peritidal
	Gal	grainstone/packstone with anhydrite laths	LFA 6: Peritidal

OTHER			
	Icg	intraclast conglomerate	LFA 6: Peritidal
	Brca	breccia	LFA 2: Slope & LFA 7: Supratidal/ Restricted
	Tep	tepee	LFA 7: Supratidal/Restricted
	Pis	pisolite	LFA 7: Supratidal/Restricted
	Tfa	tufa	LFA 7: Supratidal/Restricted
	Sm	siltstone or carbonate-cemented siltstone	LFA 6: Peritidal & LFA 7: Supratidal/Restricted
	Pss	quartz rich packstone	LFA 6: Peritidal & LFA 7: Supratidal/Restricted
	Ss	sandstone	LFA 6: Peritidal & LFA 7: Supratidal/Restricted

Figure 5.19: Grainstone and other lithofacies key

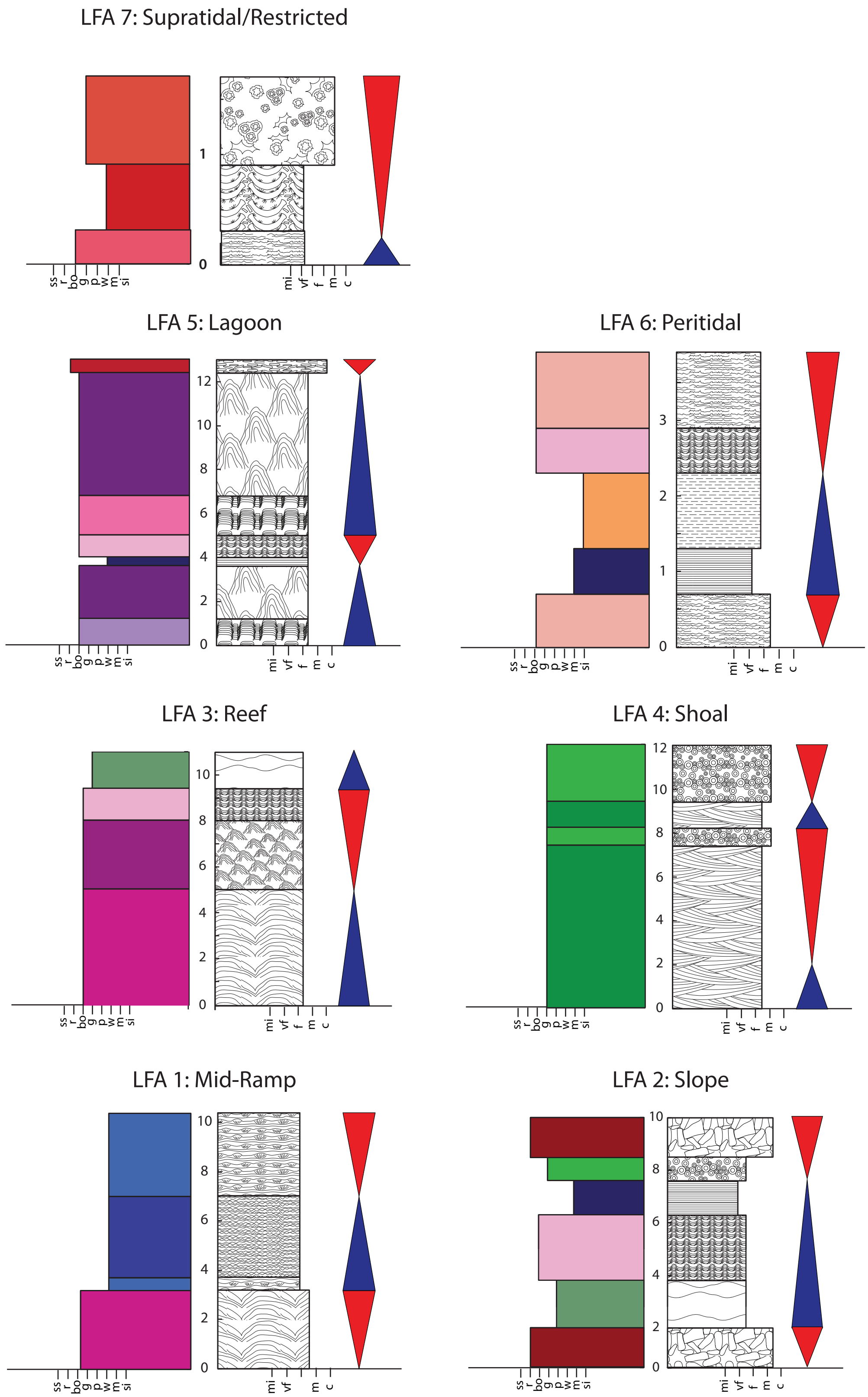

Figure 5.20: Representative parasequences from each LFA showing transgressive and regressive components.

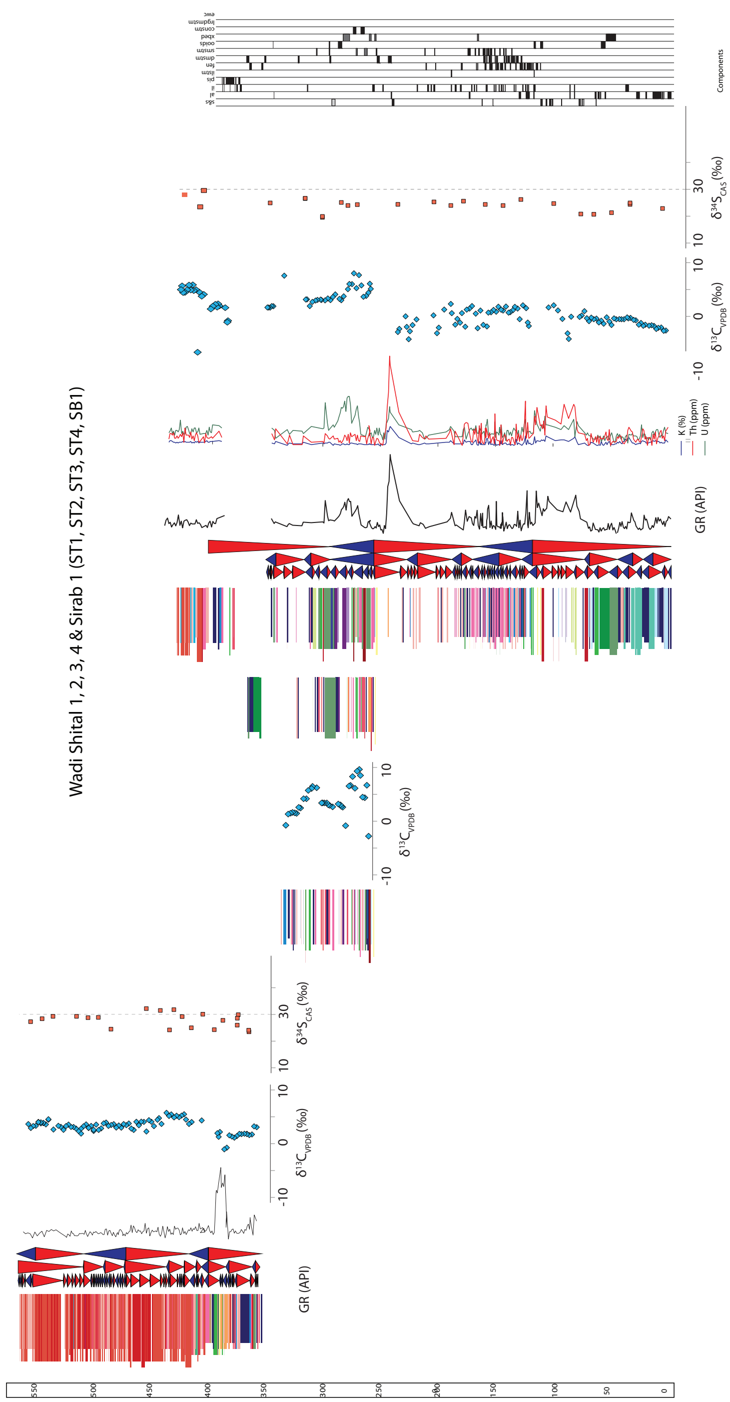

Figure 5.21: Sequence stratigraphic model for Wadi Shital and Sirab (ST1, 2, 3, 4 and SB1). Lithostratigraphy is shown as well as parasequence, parasequence set and sequence stacking patterns, total gamma ray, spectral gamma ray, $\delta^{13}C$, $\delta^{34}S$, components arranged by water depth (left being shallowest).

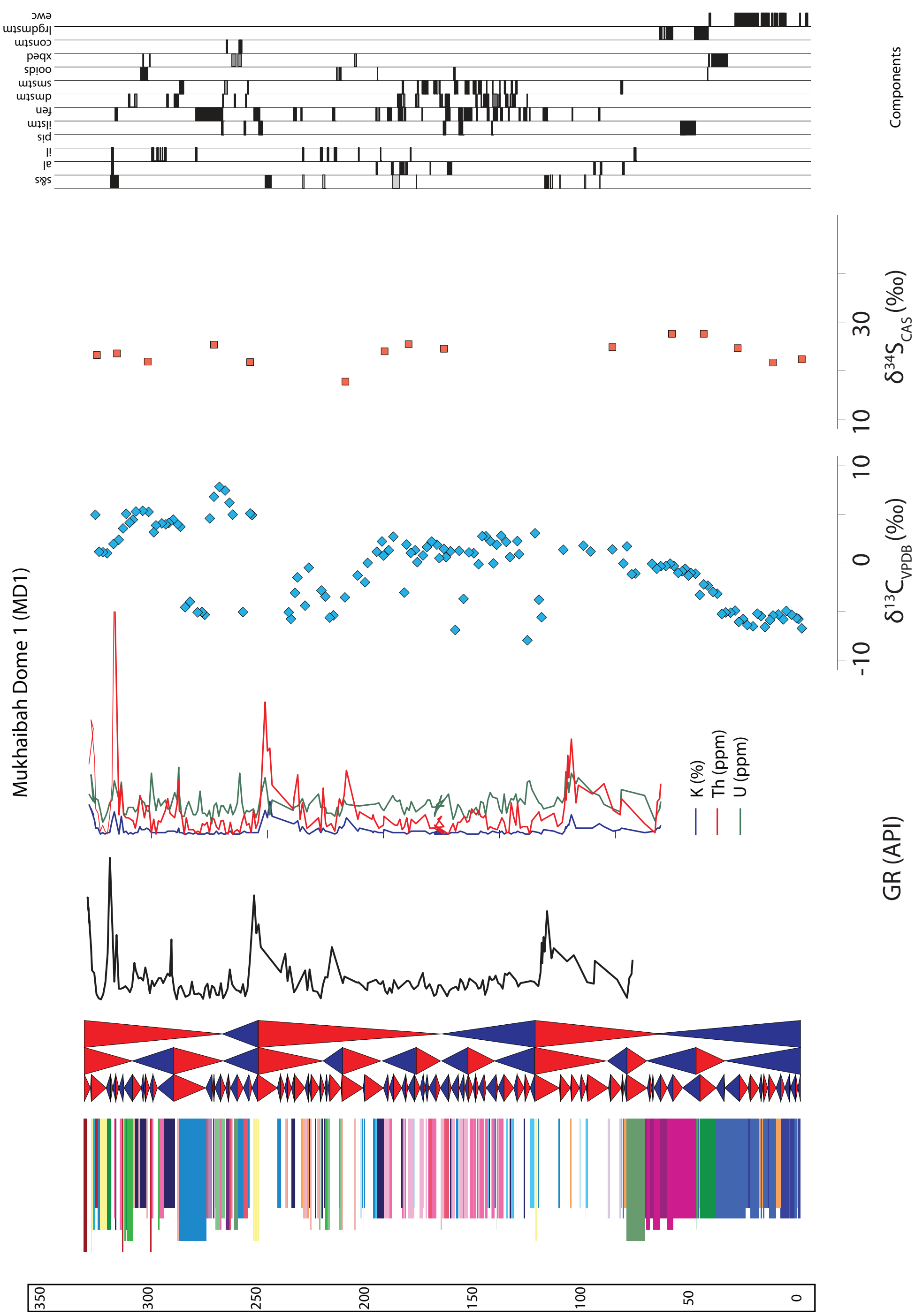

Figure 5.22: Sequence stratigraphic model for Mukhaibah Dome (MD1). Lithostratigraphy is shown as well as parasequence, parasequence set and sequence stacking patterns, total gamma ray, spectral gamma ray, δ^{13}C, δ^{34}S, components arranged by water depth (left being shallowest).

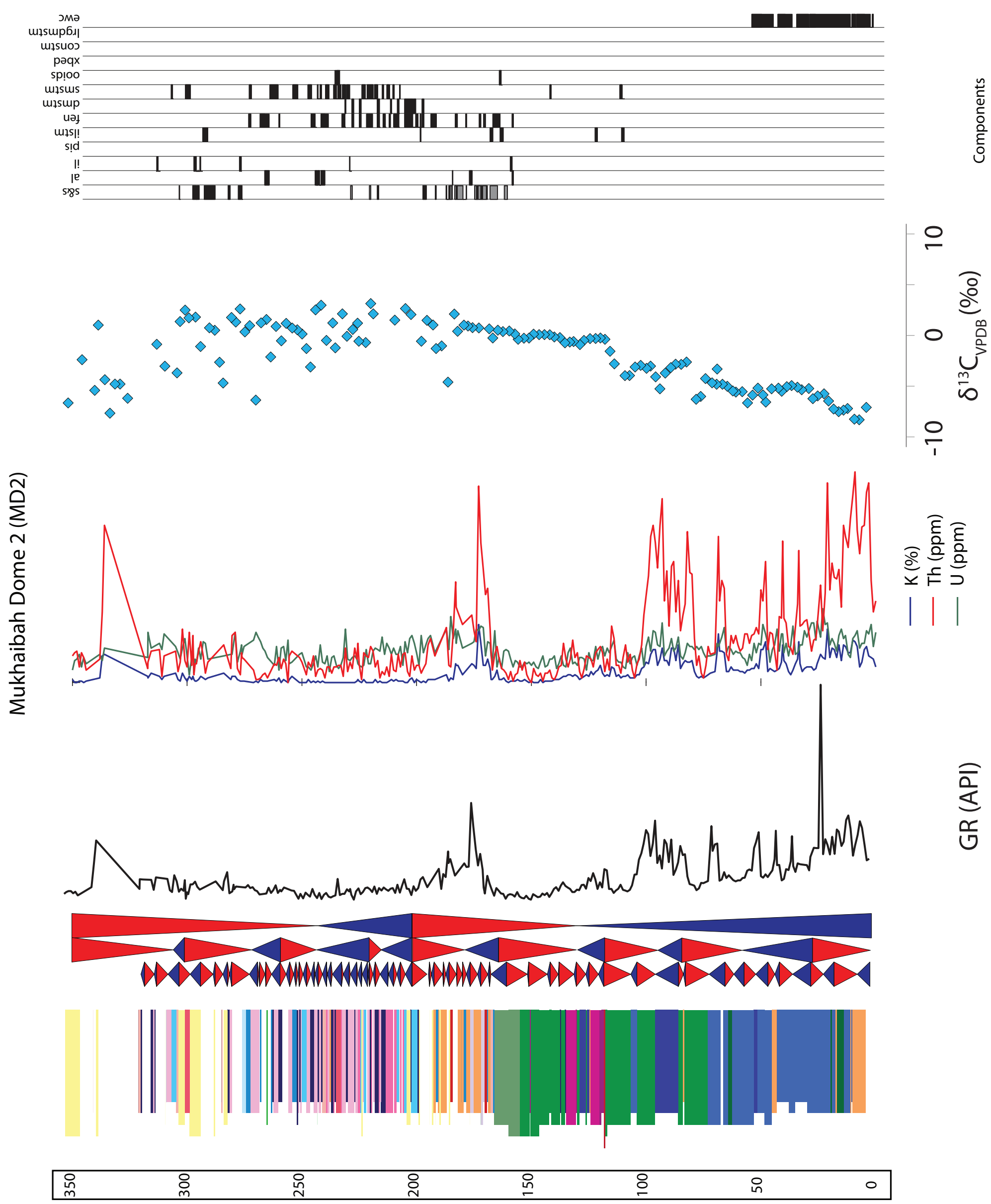

Figure 5.23: Sequence stratigraphic model for Mukhaibah Dome (MD2). Lithostratigraphy is shown as well as parasequence, parasequence set and sequence stacking patterns, total gamma ray, spectral gamma ray, δ^{13}C, δ^{34}S, components arranged by water depth (left being shallowest).

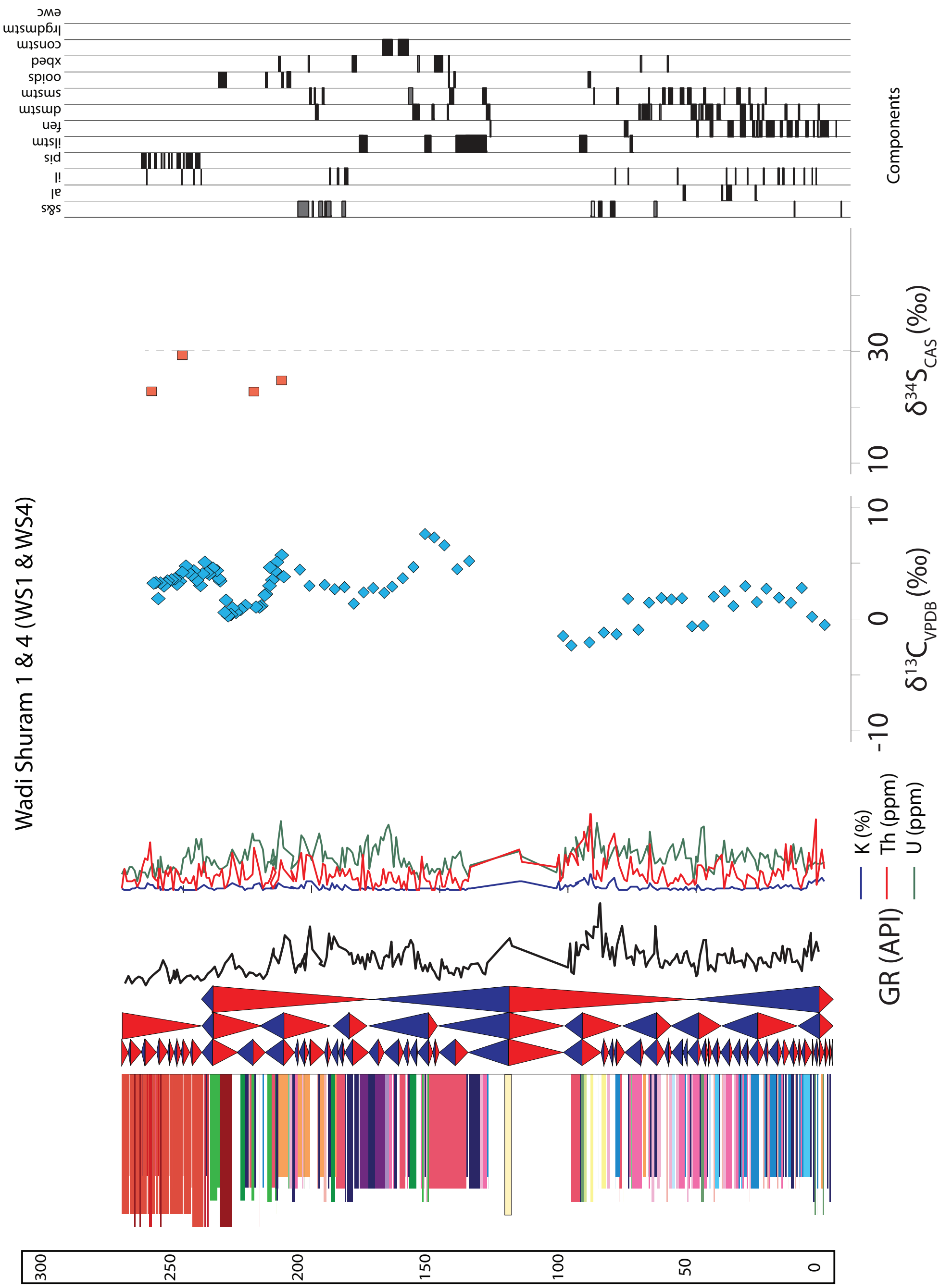

Figure 5.24: Sequence stratigraphic model for Wadi Shuram (WS1 and WS4). Lithostratigraphy is shown as well as parasequence, parasequence set and sequence stacking patterns, total gamma ray, spectral gamma ray, δ^{13}C, δ^{34}S, components arranged by water depth (left being shallowest).

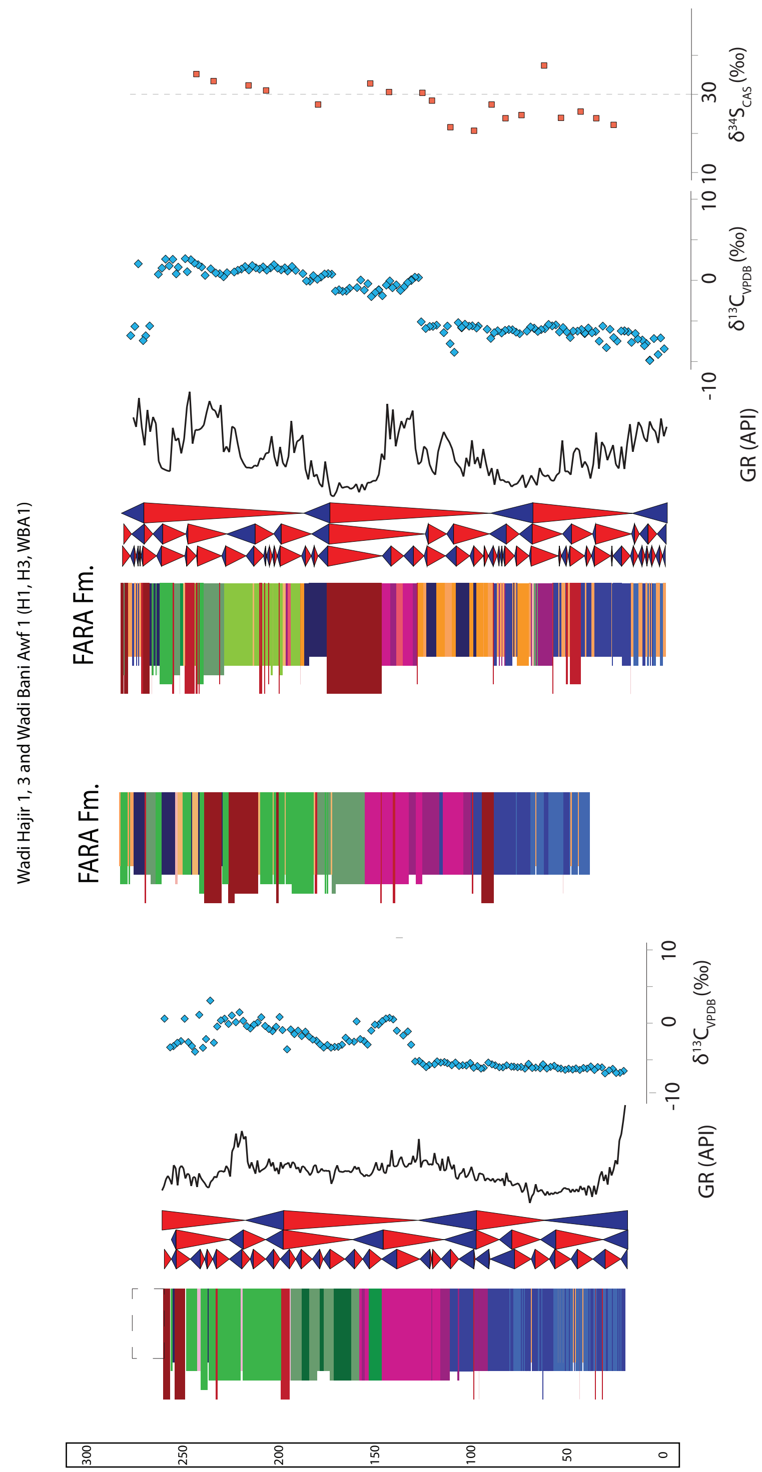

Figure 5.25: Sequence stratigraphic model for Wadi Hajir and Wadi Bani Awf (H1, H3, WBA1). Lithofacies are shown as well as parasequence, parasequence set and sequence stacking patterns, total gamma ray, δ^{13}C and δ^{34}S.

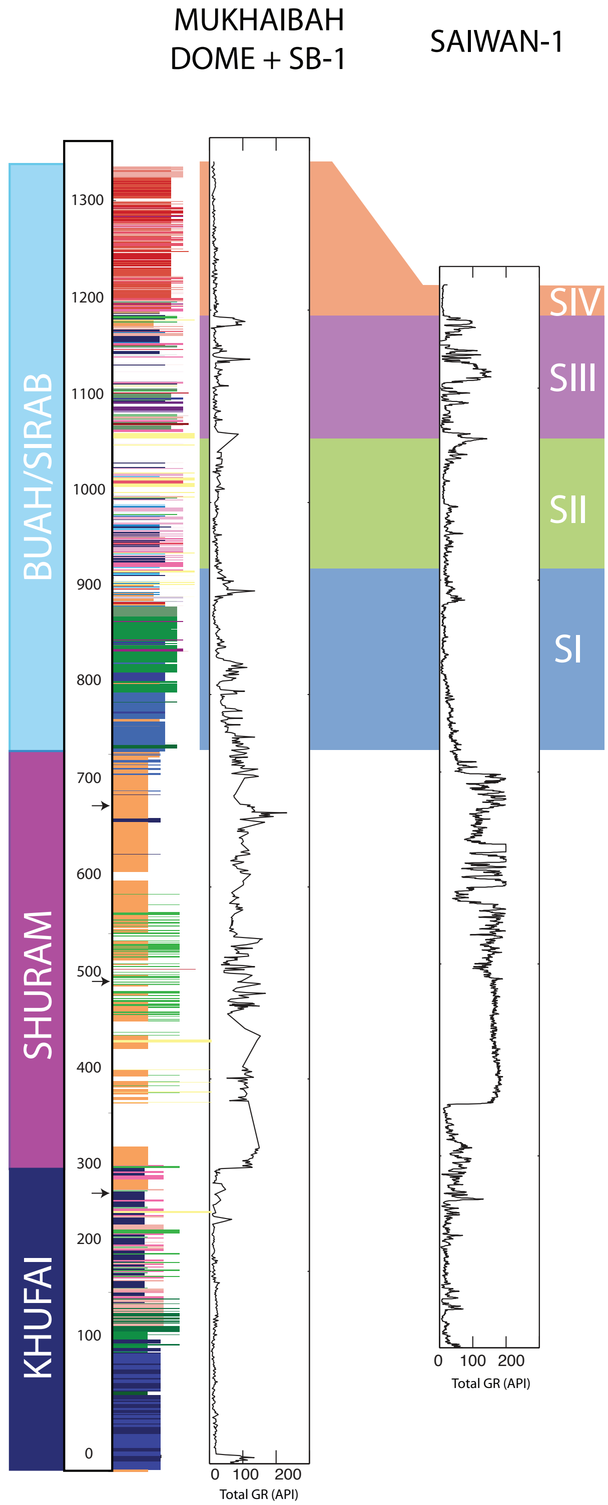

Figure 5.26: Correlation between a composite section of the Nafun Group from the Huqf outcrop area with the closest subsurface well, SWN1.

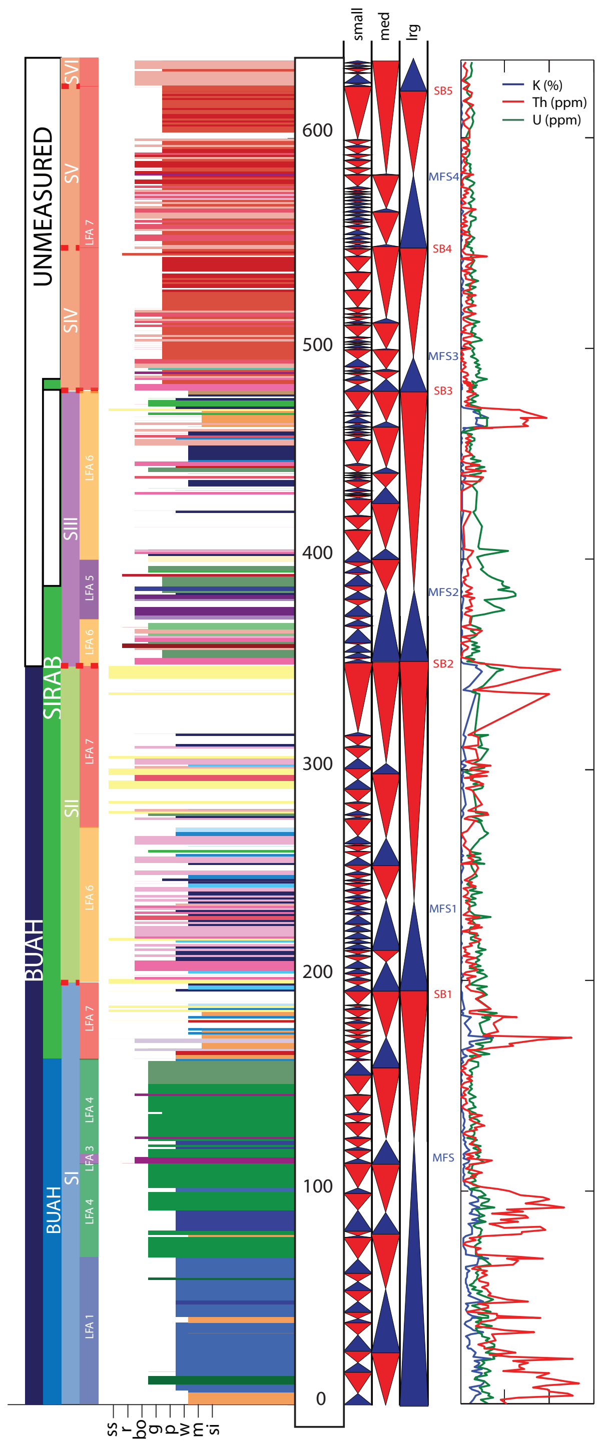

Figure 5.27: Composite stratigraphic section of the Buah and Sirab formations (Sequences I, II, III, IV, V) in the Huqf Outcrop Area. The composite section includes individual sections MD-2, ST-1 and SB-1. Plotted are lithofacies color, lithofacies association, small, medium and large transgressive-regressive cycles, and spectral GR measurements (K, %; U, ppm; Th, ppm). The sequence boundaries are designated as SB1, SB2, SB3 and SB4.

platform sediments of the Huqf Outcrop Area. In the Oman Mountains, where most of the deposits formed on the slope, this level of cyclicity is much more challenging to identify. While there are significant horizons including erosional surfaces and thick slope breccias, it is difficult to relate these horizons to relative eustatic change as they may also result from internal dynamics including slope failure or earthquakes unrelated to relative eustacy [59].

We have identified 4-5 sequences within the carbonate stratigraphy post-dating the Shuram Formation in the Huqf Outcrop Area:

Sequence 1–The first sequence includes the Shuram Formation and lowermost mid-ramp lithofacies association of the Buah Formation. The siliciclastics of the Shuram Formation shallow into crinkly laminite and edgewise conglomerate lithofacies. In Wadi Hajir in the Oman Mountains, there is a significant erosional surface that cuts down into the lower Buah crinkly laminates and edgewise conglomerates. This surface is filled in with breccias, grainstone and stromatolite boundstone. This erosional surface likely correlates with the surface the stromatolite reef facies sits on and may be equivalent to the erosional surfaces in the Johnnie and Wonoka formations (Fig. 5.30) [60, 61, 62, 63]. These three erosional surfaces from the Wonoka, Johnnie and Buah formations occur at a similar place within the isotopic recovery of the Shuram Excursion (see below). The reef lithofacies association shallows into shoal and lagoonal lithofacies associations. We define a single sequence for the previously defined Buah Formation and the 'Ramayli Member' of the Sirab Formation [11, 15, 10, 5, 4]. The distinctive surface in the Oman Mountains may mark a sequence boundary but we've currently grouped these two potential sequences into one. Unlike previous researchers, we find no evidence for a significant hiatus at the shoal crest. Instead, this stratigraphy can be related through one shallowing upwards sequence and a change in depositional environments across the platform. Just before the sequence boundary at the transition from lagoonal to peritidal lithofacies association (SB1), there is an increase in evaporite mineral deposition.

Sequence 2—The second sequence is characterized by a small amount of flooding and aggradation of a dominantly peritidal lithofacies association before the progradation of lagoonal facies. This sequence was previously defined as the 'Lower Shital Member' of the Sirab Formation [4, 5]. The sequence boundary (SB2) is characterized by increasingly restrictive and evaporitic lagoonal facies.

Sequence 3—The third sequence begins with a regional transgressive sandstone bed. Above the sandstone the carbonates are characterized by a significant and rapid flooding through peritidal lithofacies into lagoonal platform top *conophyton* reefs. The *conophyton* reefs are overlain by shallowing lagoonal facies that end in a significant sequence boundary (SB3) with localized karst development and tufa deposition.

Sequence 4—The predominantly supratidal deposits overlying SB3 are composed of vertically aggrading tepee-pisolite deposits that may contain cryptic sequence boundaries; however, these did not manifest themselves clearly in outcrop exposures. This sequence was previously termed the 'Aswad Member', and described as a shallow subtidal oncolite grainstone to thrombolite shoal facies [5, 4]. This sequence is much thicker than the previously measured ~ 5 meters, and we do not agree with the previous interpretation of depositional environment. Instead, we prefer an interpretation of supratidal deposits forming on the shelf crest because of the structures and lithofacies present—tepees, pisoids, and irregular laminites. Previously undescribed facies outcropping near Bantawt are likely time equivalent because they overlie sequence 3 and may be salt collapse breccias from more restricted lagoonal environments (Fig. 5.13).

5.7 Geologic mapping

Results from mapping the five major sequences defined within the Buah and Sirab formations across the Huqf Outcrop Area are shown in Figure 5.28. The structural anticlines and synclines control the areal extent of each sequence. The five sequences post-dating the Shuram Formation tend to form synclinal folds while the Khufai Formation forms steeply dipping anticlines. The synclines

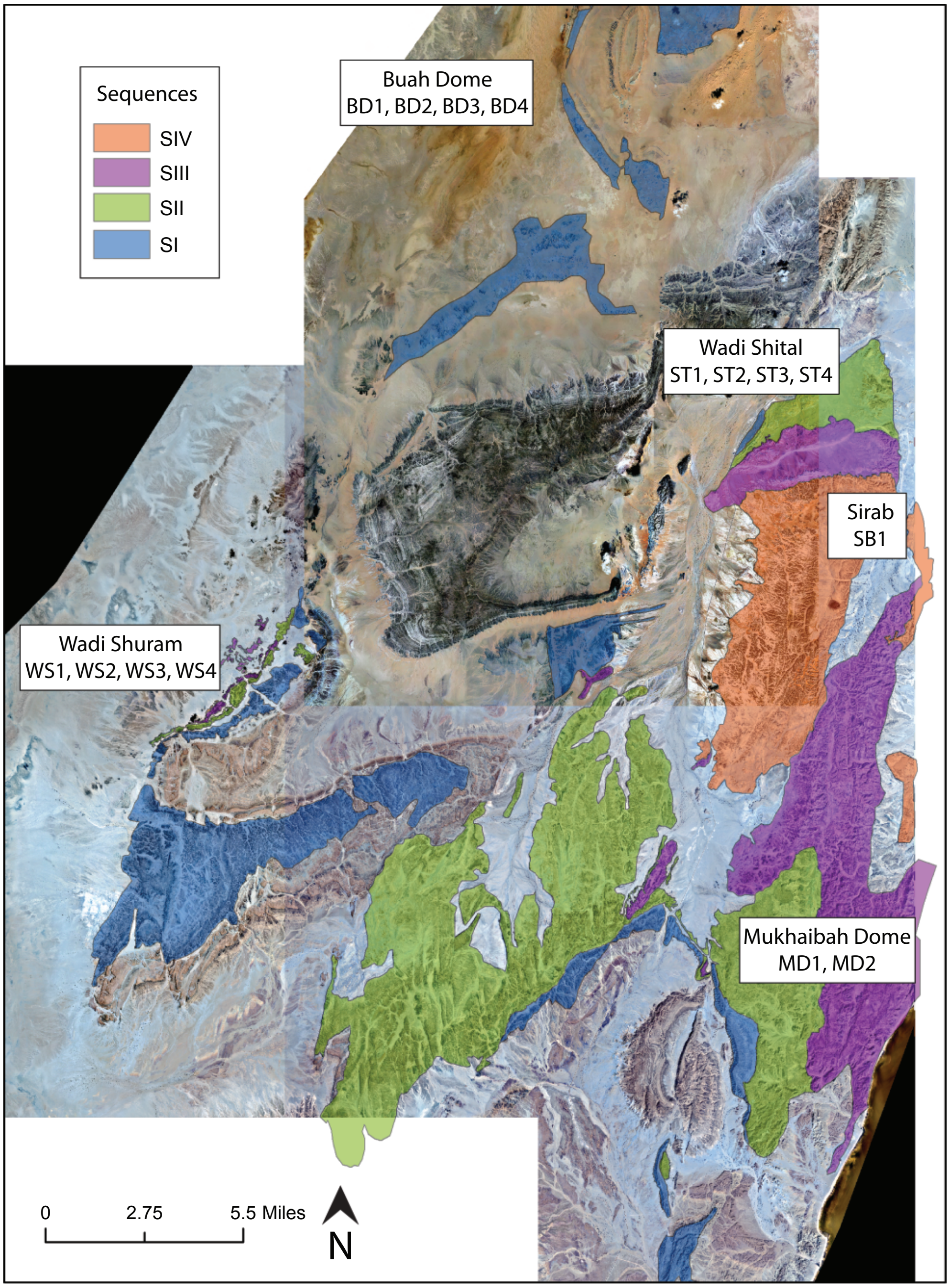

Figure 5.28: Revised geologic map of the Nafun Group in the Huqf Outcrop Area with sequences I, II, III and IV mapped of the Buah and Sirab formations.

dip shallowly and cover much of the Huqf Outcrop Area. Most of the outcrop exposures of the youngest strata of sequence 4 are exposed best closer to the coast near Sirab and Bantawt with smaller exposures present on the western edge of the Huqf outcrop area at Wadi Shuram.

Results from mapping the structures within the Buah Formation in the Oman Mountains are shown in Figure 5.29. Previous interpretations of the significant facies differences in the Buah Formation exposed in Wadi Hajir compared to Wadi Bani Awf suggested a down dropped graben forming between the shallower facies in Wadi Hajir and more distal facies in Wadi Bani Awf within a distance of 7 km [11, 15]. Based on field observations (Fig. 5.30A,B) and Quickbird imaging, we propose instead that a series of low angle thrust faults has replicated the Buah Formation at least four times. The most proximal thrust sheet is the first block in Wadi Hajir while the most distal thrust sheet is the block in Wadi Bani Awf that contains the Fara Formation. Unlike previous geologic maps (e.g., [15]) that have continuous outcrop exposure from Wadi Bani Awf to Wadi Hajir, in reality the Buah Formation is thrust along the less resistant Shuram Formation and these outcrop areas have four to five major faults dissecting them. This replication of the section actually provides a powerful opportunity of sampling more of the slope to basin transition by studying the section preserved in each successive fault block.

5.8 Depositional model and regional correlation

From our facies observations and sequence stratigraphic model, we constructed a model of carbonate platform evolution during Buah-Ara time. The model was developed based on observations from the sedimentology and stratigraphy exposed in the Oman Mountains, the Huqf Outcrop Area and subsurface cores from the South Oman Salt Basin, the Eastern Flank and the Central Oman High to best approximate changes across all of Oman (Fig. 5.31).

The transition from the siliciclastic dominated Shuram Formation to the mid-ramp facies of the lower Buah Formation is gradual. These laterally continuous

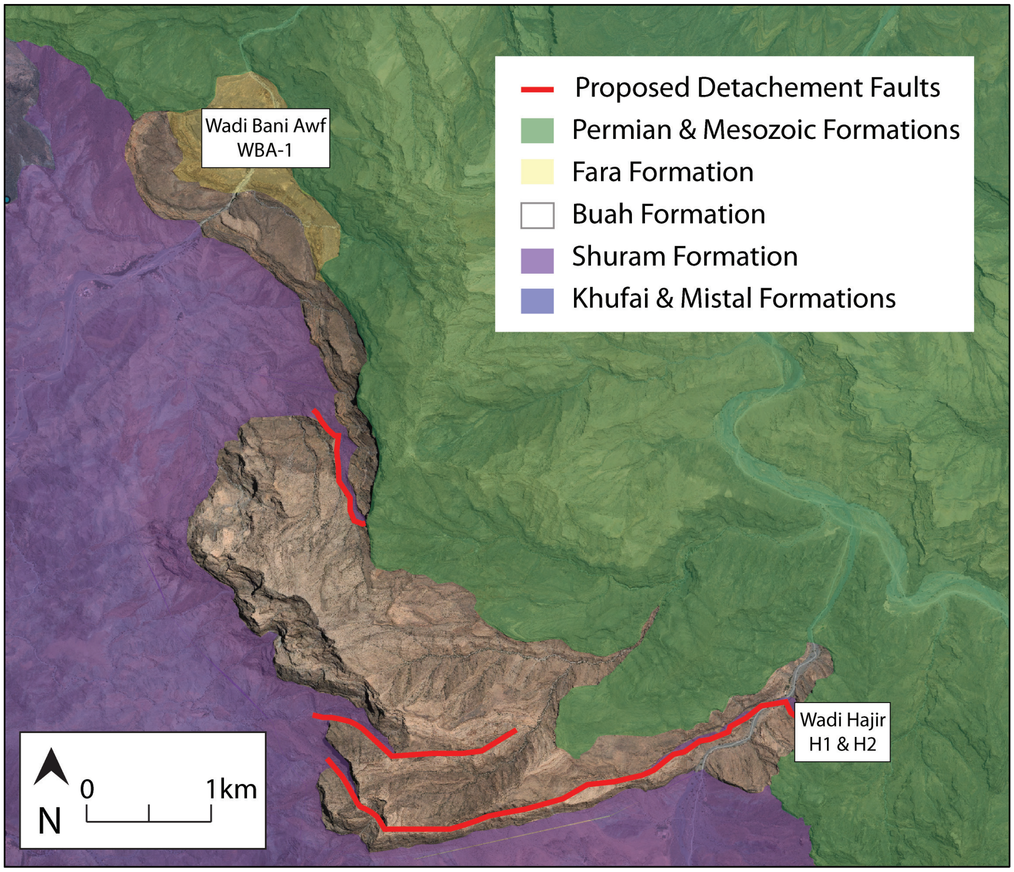

Figure 5.29: Replication of the Buah Formation in the Oman Mountains controlled by low angle thrust faults.

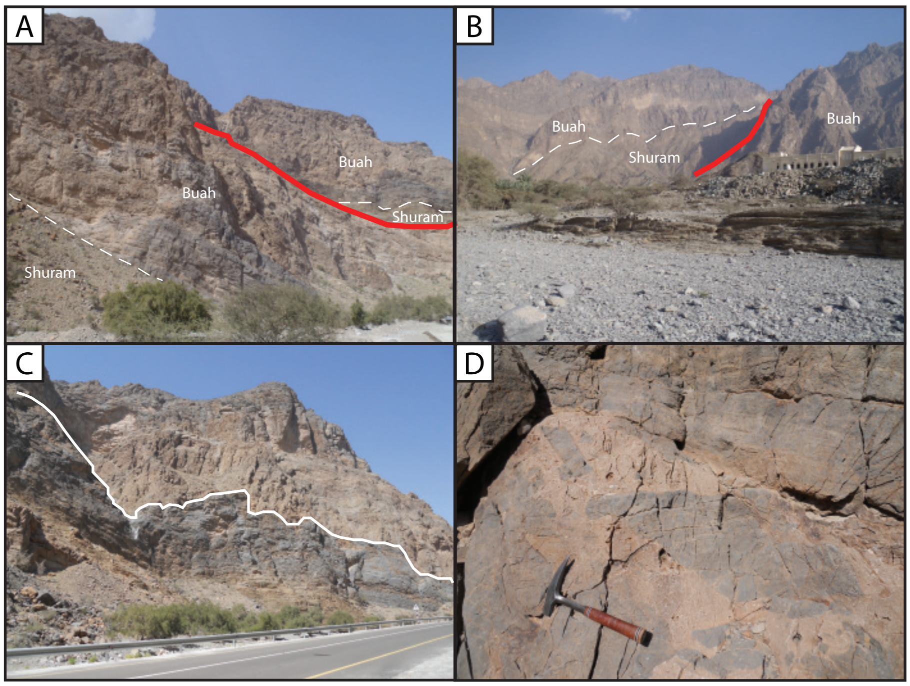

Figure 5.30: Outcrop images from the Buah Formation in the Oman Mountains. A Thrust fault and section replication in Wadi Hajir. B Thrust Fault and section replication in Wadi Bani Awf. The main section expose near the road is completely truncated by the Permian unconformity. C A surface within the lower Buah with significant erosion on it. In Wadi Hajir this surface can cut down $\sim$ 30 m into the edgewise conglomerate facies. The sediments filling this erosional surface include breccias near the base, grainstone, and stromatolitic boundstone. D a representative example of a breccia infilling the erosional unconformity.

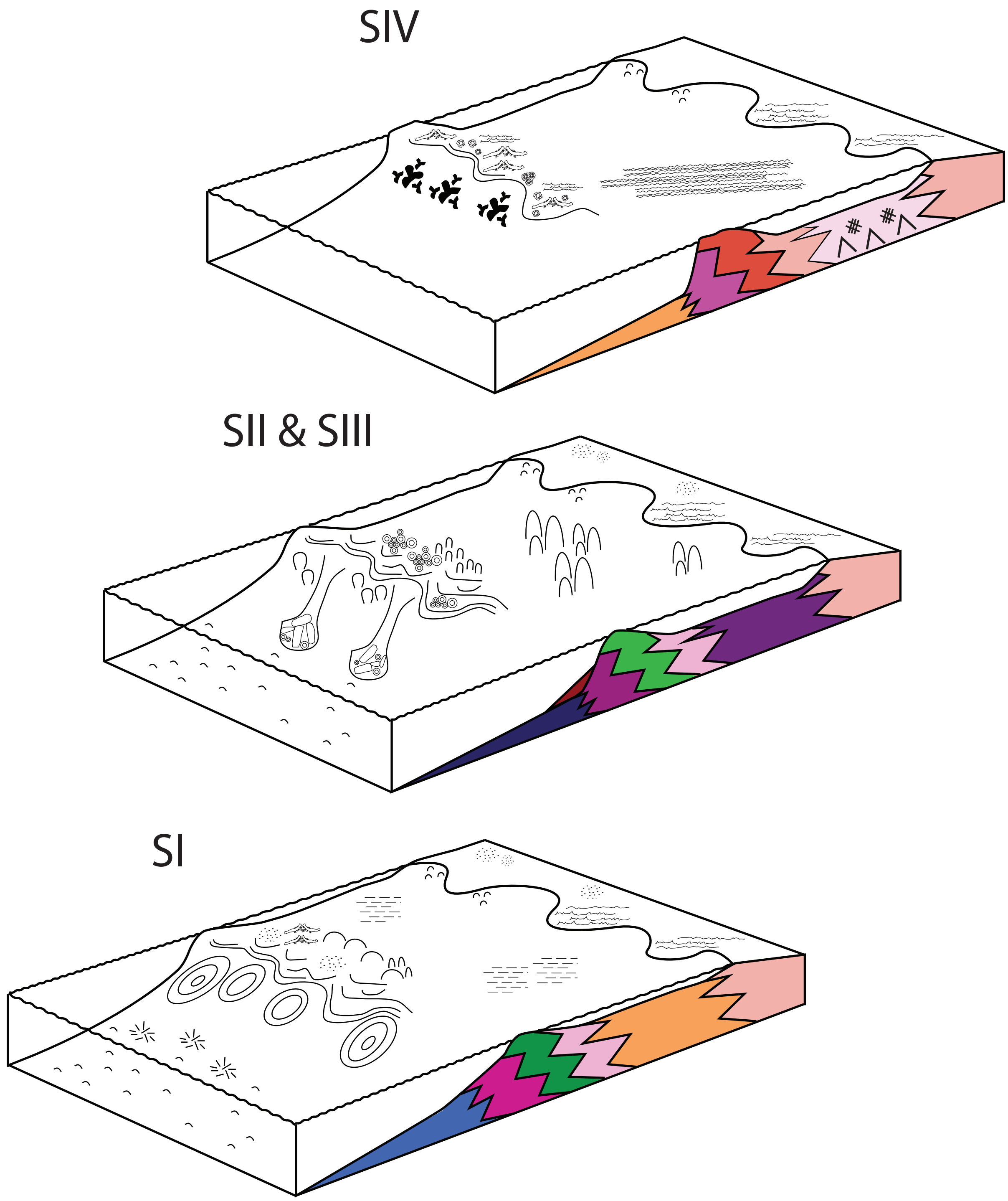

Figure 5.31: Depositional models for each of the major sequences which generally depict a shallowing upward trend and steepening of the platform. The dominate facies and their position on the platform are indicated.

shallow-water, variable energy deposits are capped by reefal stromatolites that transition the broad ramp morphology into a steep sided carbonate platform morphology (Fig. 5.31). The flat-topped platform morphology that develops across Oman is a classic morphology with slope deposits, a reef, grainstone shoals and inner platform lagoonal and peritidal deposits (e.g., the Capitan Reef Complex in the Guadalupe Mountains [64]). The change in platform morphology is supported by the expansive lagoonal and peritidal lithofacies associations found in the Huqf outcrop area and the slope breccias found in the Oman Mountains as well as analogous subsurface core lithofacies (i.e., ZL1 and SWT8). The inner platform and slope deposits can both be siliciclastic rich and evaporative. There are multiple progradational, aggradational and retrogradational cycles that result in a migrating shoreline and repetitive stacking of the shallow-water lithofacies associations in the Huqf Outcrop Area. The orientation of the main platform edge was likely NE-SW based on paleocurrent tidal current indicators [8, 11, 28].

Based on the sequence stratigraphic model, lithofacies patterns, and gamma ray log character we interpret the sequence boundary with karst development in the Huqf Outcrop Area (SB3) as the Buah-Ara Boundary. Thus the transition to a flat-topped platform with evaporative siliclastic rich lagoonal deposits begins in the Buah Formation. The Buah Formation is likely to be characterized by variable siliciclastic content in the subsurface depending on where on the platform it is penetrated. Additionally the three sequences within the Buah Formation will results in progradation and retrogradation of lithofacies associations across the platform. The interpreted Buah-Ara Boundary at SB3 coincides with a significant depositional shift to a dominantly supratidal lithofacies association in the Huqf Outcrop Area. A localized karst breccia capped by a thick sequence of tepee structures, pisoids and irregular laminites ($>$ 150 meters thick) suggests the development of a rimmed platform. Similar facies with tepee structures and pisoids in the subsurface cores of the Birba Formation in SWN1 and the Eastern Flank suggest this tepee-pisolite rim extended along the entire platform crest. The development of the tepee-pisolite complex coincided with thick inner platform lagoonal deposits prone to restriction and evaporite deposition of the traditional Ara Group cycles of the South Oman Salt Basin and the Ghaba Salt Basin [7, 29, 30]. Gamma ray logs from the Birba Formation across Oman suggest a shut off of siliciclastic input to the platform as a whole. During this time interval the main reef facies likely transitioned to thrombolite boundstone as evidenced by cored intervals just off the crest of the Eastern Flank (Fig. 5.7). These microbial boundstones with a different growth habit than stromatolites may have acted to stabilize the platform rim, decreasing the abundance of slope breccias seen in the more distal deposits of the Athel Trough and Fara Formation in the Oman Mountains.

5.9 Chemostratigraphy

5.9.1 Carbon isotopic patterns

To test the validity of using δ^{13}C for correlation across Oman in the latest Precambrian we have overlain the isotopic data on our sequence stratigraphic model. The carbon isotopic pattern is laterally consistent from the Huqf Outcrop Area to the Oman Mountains when the sections are aligned based on the sequence stratigraphic architectural described above. Sequence 1 is characterized by a general recovery from the negative Shuram Excursion. There is a positive excursion from values of $\sim$ -8‰ to $\sim$ 0‰ in the reefal stromatolite lithofacies association. Values continue to increase through the grainstone shoal and lagoonal sediments. The δ^{13}C values immediately prior to SB1 become negative (-4‰) although the degree of depletion is variable and most extreme in the restricted lagoonal facies. A significant shift to positive values occurs above SB2 with δ^{13}C values reaching +7–8‰VPDB. This positive excursion has two smaller excursions within it that are preserved within sequence 3 whether there was significant accommodation space (ST1) or minimal accommodation space (ST2). The magnitude of this excursion is similar to values documented in the Nama Group of Namibia (5-6‰) and this excursion found in the subsurface well MQ1 has previously been correlated with the excursion in the Nama Group [42, 39]. Above

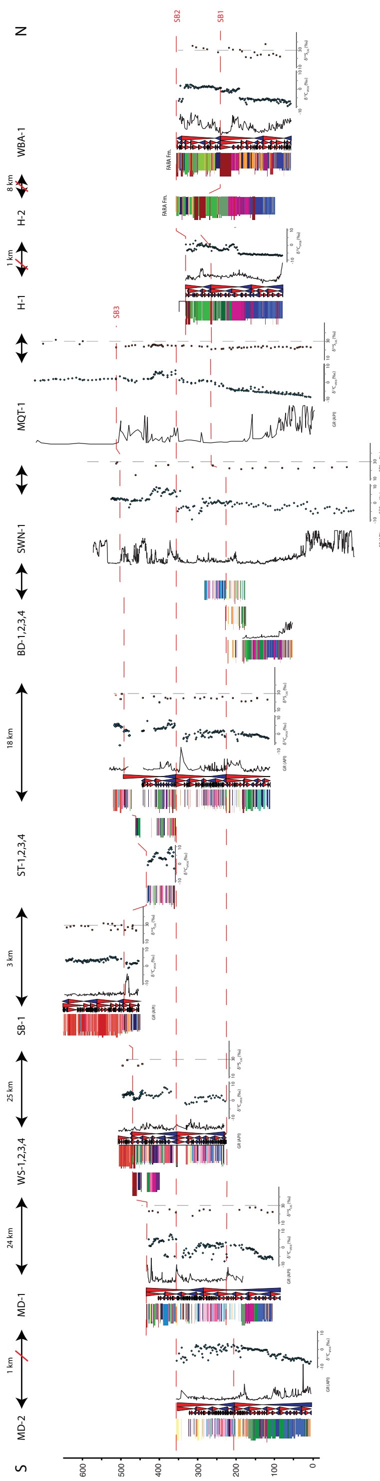

Figure 5.32: Correlation Panel for central to northern Oman.

SB3 the isotopic composition of sequence 4 is flat at $\sim 2‰$. The δ^{13}C isotopic composition and gamma ray log character of each sequence in consistent from the Huqf to two subsurface wells to the north, SWN1 and MQT1. Additionally, the flat δ^{13}C and clean gamma ray log character of sequence 4 in all three locations is similar to the Birba Formation (A1–A3) along the Eastern Flank.

5.9.2 Sulfur isotopic pattern

The two models most recently published for the stratigraphy in Central Oman are in disagreement because [3] proposes the $\delta^{34}S_{CAS}$ isotopic composition of the proposed 'Sirab Formation' is 'Nafun Group' in character and $\sim$ 20–25‰. In contrast, δ^{34}S results from definitive Ara Group samples from the SOSB are $\sim$ 30-40‰ [3]. To address whether the $\delta^{34}S_{CAS}$ isotopic composition can be used to distinguish the 'Nafun Group' from the 'Ara Group', we have expanded the $\delta^{34}S_{CAS}$ record of this time interval in Oman and have overlain the data on our sequence stratigraphic model. As demonstrated above this model yields consistent δ^{13}C compositions across Oman for a given time horizon. The sulfur isotopic composition of sequences 1–3 in Central Oman are near constant at $\sim$ 25‰ similar to previously analyzed samples [3]. The previously unanalyzed stratigraphy of sequence 4, which we correlate with the Birba Formation, is heavier than underlying sediments and has an average of +30‰ but can reach values as high as 32‰. While this isotopic composition is not as heavy as some Ara Group samples from subsurface wells from the SOSB [3], it is very similar to the baseline $\delta^{34}S_{CAS}$ composition of well SBSB1 which is definitively A0–A3 in age because *Cloudina* grainstone facies are associated with the thrombolite boundstone observed in cores.

These results suggest the shift to heavier $\delta^{34}S_{CAS}$ values associated with the Ara Group locally and with the Precambrian-Cambrian transition globally is a consistent trend [16, 18, 20, 17, 19, 21]. However, the δ^{34}S isotopic composition does appear to vary in absolute magnitude from the Eastern Flank and Central Oman High to the South Oman Salt Basin. This suggests pyrite burial in deeper basinal environments like the Athel Trough within the South Oman Salt Basin is likely important in driving local enrichment in the SOSB.

5.10 Conclusions

To address competing models for correlation of the carbonates from the latest Precambrian of Oman, we used a combined approach to build a sequence stratigraphic framework for the carbonates deposited in Central Oman, the Oman Mountains and the subsurface Eastern Flank of the South Oman Salt Basin and Central Oman High.

The carbonates deposited in the latest Precambrian of Oman document the evolution of a microbially dominated platform from a ramp morphology to a flat-topped platform morphology. Our results indicate the platform becomes increasingly restricted approaching the Precambrian-Cambrian boundary, coincident with a shut off of siliciclastic material, and a wide rimmed tepee-pisolite complex develops on the platform crest while evaporites and microbial carbonates are deposited in the inner platform.

The chemostratigraphic pattern of these carbonates agrees well when sections are aligned using key sequence stratigraphic surfaces. The δ^{13}C composition of these carbonates varies temporally and the magnitude of depletion or enrichment is broadly consistent across Oman for a given time interval. The relationship between excursions and major sequence boundaries suggests a link between the carbon cycle and carbonate platform cyclicity. The $\delta^{34}S_{CAS}$ composition does increase in the late Precambrian across Oman but the magnitude of the increase is not constant.

Our work would suggest the majority of the newly defined 'Sirab Formation' is in actuality part of the Buah Formation, a correlation model that agrees well with early work in the region [8, 12, 13, 14]. The tepee-pisolite complex of sequence 5 likely correlates with the Birba Formation of the Eastern Flank and Northern Carbonate Domain.

5.11 Acknowledgements

We would like to thank Said Al Balushi for help in the field with outcrop gamma ray logging. We would also like to thank multiple people at Petroleum Development Oman for helpful conversations including Gideon Lopes Cardozo, Gordon Forbes, Bill Wilks, Joachim Amthor, Sven Scholten, Irene Gomez Perez, Suleiman Farqani, Badar Baloushi, Aly Brandenburg, Richard Hallet, Zuwena Al-Rawahi, and Massimo Mauro. Magdalena Osburn and Jena Johnson assisted with field work during the winter 2011 and 2012 field seasons. Alexandra Ruiz, Ellie Rae Hoffman, Steve Bates and Tim Lyons helped with sulfur isotope sample preparation and completed the sulfur isotope analysis. We would like to thank Petroleum Development Oman for logistical support and funding for analytical work. A National Science Foundation Graduate Research Fellowship was provided to K. Bergmann and the NASA Astrobiology Institute and the Agouron Institute partially funded the research.

References

[1] S.A. Bowring, J.P. Grotzinger, D.J. Condon, J. Ramezani, M.J. Newall, and P.A. Allen. Geochronologic constraints on the chronostratigraphic framework of the Neoproterozoic Huqf Supergroup, Sultanate of Oman. *American Journal of Science*, 307(10):1097–1145, 2007.

[2] P.A. Allen. The Huqf Supergroup of Oman: Basin development and context for Neoproterozoic glaciation. *Earth-Science Reviews*, 84(3-4):139–185, 2007.

[3] D.A. Fike and J.P. Grotzinger. A paired sulfate-pyrite delta S-34 approach to understanding the evolution of the Ediacaran-Cambrian sulfur cycle. *Geochimica Et Cosmochimica Acta*, 72(11):2636–2648, 2008.

[4] S.E.P. Gold. *Stratigraphy and correlation of the Sirab Formation, Al Huqf Area, with the subsurface Ara Group play systems of Oman*. Ph.D. thesis, 2009.

[5] C.J. Nicholas and S.E.P. Gold. Ediacaran-Cambrian Sirab Formation of the Al Huqf region, Sultanate of Oman. *Geoarabia*, 17(1):49–98, 2012.

[6] B.W. Mattes and S.C. Morris. Carbonate evaporite deposition in the Late Precambrian - Early Cambrian Ara Formation of Southern Oman. *Geology and Tectonics of the Oman Region*, 49:617–636 845, 1990.

[7] S. Schroder, B.C. Schreiber, J.E. Amthor, and A. Matter. A depositional model for the terminal Neoproterozoic Early Cambrian Ara Group evaporites in south Oman. *Sedimentology*, 50(5):879–898, 2003.

[8] G.M.E. McCarron. *The sedimentology and chemostratigraphy of the Nafun Group, Huqf Supergroup, Oman.* Ph.D. thesis, 2000.

[9] D.A. Fike. *Carbon and sulfur isotopic constraints on Ediacaran biogeochemical processes, Huqf Supergroup, Sultanate of Oman.* Ph.D. thesis, 2007.

[10] C.J. Nicholas and M. Braiser. Outcrop equivalent of the subsurface Precambrian-Cambrian Ara Group in Oman. In *4th Middle East Geosciences Conference*, volume 5, pages 151–152. GeoArabia, 2000.

[11] A. Cozzi, P.A. Allen, and J.P. Grotzinger. Understanding carbonate ramp dynamics using delta C-13 profiles: examples from the Neoproterozoic Buah Formation of Oman. *Terra Nova*, 16(2):62–67, 2004.

[12] V.P. Wright, A.C. Ries, and S.G. Munn. Intraplatformal basin-fill deposits from the Infracambrian Huqf Group, east Central Oman. *Geology and Tectonics of the Oman Region*, 49:601–616, 1990.

[13] G.E. Gorin, L.G. Racz, and M.R. Walter. Late Precambrian-Cambrian sediments of Huqf Group, Sultanate of Oman. *AAPG Bulletin*, 66(12):2609–2627, 1982.

[14] J. Dubreuilah, J.P. Platel, J. Le Metour, J. Roger, R. Wyns, F. Bechennec, and A. Berthiaux. Geological map of Khaluf: Sheet NF 40-15, explanatory notes. *Bureau de Recherches Geologiques et Minieres*, Orleans, France(Cedex 2), 1992.

[15] A. Cozzi, J.P. Grotzinger, and P.A. Allen. Evolution of a terminal Neoproterozoic carbonate ramp system (Buah Formation, Sultanate of Oman): Effects of basement paleotopography. *Geological Society of America Bulletin*, 116(11-12):1367–1384, 2004.

[16] A. Kampschulte and H. Strauss. The sulfur isotopic evolution of Phanerozoic seawater based on the analysis of structurally substituted sulfate in carbonates. *Chemical Geology*, 204(3-4):255–286, 2004.

[17] H. Strauss. The isotopic composition of sedimentary sulfur through time. *Palaeogeography Palaeoclimatology Palaeoecology*, 132(1-4):97–118, 1997.

[18] G.A. Shields, H. Strauss, S.S. Howe, and H. Siegmund. Sulphur isotope compositions of sedimentary phosphorites from the basal Cambrian of China: implications for Neoproterozoic-Cambrian biogeochemical cycling. *Journal of the Geological Society*, 156:943–955, 1999.

[19] H. Strauss. Geological evolution from isotope proxy signals - sulfur. *Chemical Geology*, 161(1-3):89–101, 1999.

[20] H. Strauss, D.M. Banerjee, and V. Kumar. The sulfur isotopic composition of Neoproterozoic to early Cambrian seawater - evidence from the cyclic Hanseran evaporites, NW India. *Chemical Geology*, 175(1-2):17–28, 2001.

[21] T. Goldberg, S.W. Poulton, and H. Strauss. Sulphur and oxygen isotope signatures of late Neoproterozoic to early Cambrian sulphate, Yangtze Platform, China: Diagenetic constraints and seawater evolution. *Precambrian Research*, 137(3-4):223–241, 2005.

[22] P.A. Allen, J. Leather, and M.D. Brasier. The Neoproterozoic Fiq glaciation and its aftermath, Huqf Supergroup of Oman. *Basin Research*, 16(4):507–534, 2004.

[23] J. Leather, P.A. Allen, M.D. Brasier, and A. Cozzi. Neoproterozoic snowball Earth under scrutiny: Evidence from the Fiq glaciation of Oman. *Geology*, 30(10):891–894, 2002.

[24] R. Rieu and P.A. Allen. Siliciclastic sedimentation in the interlude between two Neoproterozoic glaciations, Mirbat area, southern Oman: A missing link in the Huqf Supergroup? *Geoarabia*, 13(4):45–72, 2008.

[25] P.A. Allen and J. Leather. Post-Marinoan marine siliciclastic sedimentation: The Masirah Bay Formation, Neoproterozoic Huqf Supergroup of Oman. *Precambrian Research*, 144(3-4):167–198, 2006.

[26] M. Osburn, J. Grotzinger, and K. Bergmann. Facies, stratigraphy, and evolution of a Middle-Ediacaran-age carbonate ramp: Khufai Formation, Sultanate of Oman. *AAPG Bulletin*, inpress.

[27] E. Le Guerroue, P.A. Allen, and A. Cozzi. Parasequence development in the Ediacaran Shuram Formation (Nafun Group, Oman): high-resolution stratigraphic test for primary origin of negative carbon isotopic ratios. *Basin Research*, 18(2):205–219, 2006.

[28] E. Le Guerroue, P.A. Allen, and A. Cozzi. Chemostratigraphic and sedimentological framework of the largest negative carbon isotopic excursion in Earth history: The Neoproterozoic Shuram Formation (Nafun Group, Oman). *Precambrian Research*, 146(1-2):68–92, 2006.

[29] S. Schroder, B.C. Schreiber, J.E. Amthor, and A. Matter. Stratigraphy and environmental conditions of the terminal Neoproterozoic-Cambrian period in Oman: evidence from sulphur isotopes. *Journal of the Geological Society*, 161:489–499, 2004.

[30] S. Schroder, J.P. Grotzinger, J.E. Amthor, and A. Matter. Carbonate deposition and hydrocarbon reservoir development at the Precambrian-Cambrian boundary: The Ara Group in South Oman. *Sedimentary Geology*, 180(1-2):1–28, 2005.

[31] A.J. Kaufman and A.H. Knoll. Neoproterozoic variations in the C-isotopic composition of seawater - stratigraphic and biogeochemical implications. *Precambrian Research*, 73(1-4):27–49, 1995.

[32] A.H. Knoll, J.P. Grotzinger, A.J. Kaufman, and P. Kolosov. Integrated approaches to terminal Proterozoic stratigraphy - an example from the Olenek Uplift, Northeastern Siberia. *Precambrian Research*, 73(1-4):251–270, 1995.

[33] F.A. Corsetti, S.M. Awramik, D.W. Pierce, and A.J. Kaufman. Using chemostratigraphy to correlate and calibrate unconformities in Neoprotero-

zoic strata from the southern Great Basin of the United States. *International Geology Review*, 42(6):516 – 533, 2000.

[34] G.P. Halverson, P.F. Hoffman, D.P. Schrag, A.C. Maloof, and A.H.N. Rice. Toward a Neoproterozoic composite carbon-isotope record. *Geological Society of America Bulletin*, 117(9-10):1181–1207, 2005.

[35] G.P. Halverson, B.P. Wade, M.T. Hurtgen, and K.M. Barovich. Neoproterozoic chemostratigraphy. *Precambrian Research*, 182(4):337–350, 2010.

[36] A.H. Knoll. Learning to tell Neoproterozoic time. *Precambrian Research*, 100(1-3):3–20, 2000.

[37] A.H. Knoll, J.M. Hayes, A.J. Kaufman, K. Swett, and I.B. Lambert. Secular variation in carbon isotope ratios from upper Proterozoic successions of Svalbard and East Greenland. *Nature*, 321(6073):832–838, 1986.

[38] S.J. Burns and A. Matter. Carbon isotopic record of the latest Proterozoic from Oman. *Eclogae Geologicae Helvetiae*, 86(2):595–607, 1993.

[39] D.A. Fike, J.P. Grotzinger, L.M. Pratt, and R.E. Summons. Oxidation of the Ediacaran ocean. *Nature*, 444(7120):744–747, 2006.

[40] E. Le Guerroue, P.A. Allen, A. Cozzi, J.L. Etienne, and M. Fanning. 50 myr recovery from the largest negative delta C-13 excursion in the Ediacaran ocean. *Terra Nova*, 18(2):147–153, 2006.

[41] J.P. Grotzinger, D.A. Fike, and W.W. Fischer. Enigmatic origin of the largest-known carbon isotope excursion in Earth's history. *Nature Geoscience*, 4(5):285–292, 2011.

[42] B.Z. Saylor, A.J. Kaufman, J.P. Grotzinger, and F. Urban. A composite reference section for terminal Proterozoic strata of southern Namibia. *Journal of Sedimentary Research*, 68(6):1223–1235, 1998.

[43] J.P. Grotzinger, S.A. Bowring, B.Z. Saylor, and A.J. Kaufman. Biostratigraphic and geochronological constraints on early animal evolution. *Science*, 270(5236):598–604, 1995.

[44] J.E. Amthor, J.P. Grotzinger, S. Schroder, S.A. Bowring, J. Ramezani, M.W. Martin, and A. Matter. Extinction of *Cloudina* and *Namacalathus* at the Precambrian-Cambrian boundary in Oman. *Geology*, 31(5):431–434, 2003.

[45] J.E. Amthor, K. Ramseyer, T. Faulkner, and P. Lucas. Stratigraphy and sedimentology of a chert reservoir at the Precambrian-Cambrian boundary: the Al Shomou Silicilyte, South Oman Salt Basin. *Geoarabia*, 10(2):89–122, 2005.

[46] D.A. Fike and J.P. Grotzinger. A delta S-34(SO4) approach to reconstructing biogenic pyrite burial in carbonate-evaporite basins: An example from the Ara Group, Sultanate of Oman. *Geology*, 38(4):371–374, 2010.

[47] G.D. Love, E. Grosjean, C. Stalvies, D.A. Fike, J.P. Grotzinger, A.S. Bradley, A.E. Kelly, M. Bhatia, W. Meredith, C.E. Snape, S.A. Bowring, D.J. Condon, and R.E. Summons. Fossil steroids record the appearance of *Demospongiae* during the Cryogenian period. *Nature*, 457(7230):718–U715, 2009.

[48] J.P. Grotzinger. Evolution of Early Proterozoic passive-margin carbonate platform, Rocknest Formation, Wopmay Orogen, Northwest-Territories, Canada. *Journal of Sedimentary Petrology*, 56(6):831–847, 1986.

[49] M.C. Pope and J.P. Grotzinger. Controls on fabric development and morphology of tufas and stromatolites, uppermost Pethei Group (1.8 ga), Great Slave Lake, Northwest Canada. In J.P. Grotzinger and N.P. James, editors, *Carbonate sedimentation and diagenesis in the evolving Precambrian world*, volume Special Publication 67, pages 103–121. SEPM, 2000.

[50] M.C. Pope, J.P. Grotzinger, and B.C. Schreiber. Evaporitic subtidal stromatolites produced by in situ precipitation: Textures, facies associations, and temporal significance. *Journal of Sedimentary Research*, 70(5):1139–1151, 2000.

[51] L.C. Kah, J.K. Bartley, T.D. Frank, and T.W. Lyons. Reconstructing sea-level change from the internal architecture of stromatolite reefs: an example from the Mesoproterozoic Sulky Formation, Dismal Lakes Group, arctic Canada. *Canadian Journal of Earth Sciences*, 43(6):653–669, 2006.

[52] J. Bertrandsarfati and A. Moussinepouchkine. Evolution and environmental-conditions of *Conophyton-Jacutophyton* associations in the Atar Dolomite (Upper Proterozoic, Mauritania). *Precambrian Research*, 29:207–234, 1985.

[53] R. Assereto and C.C. Kendall. Nature, origin and classification of peritidal tepee structures and related breccias. *Sedimentology*, 24:153–210, 1977.

[54] R.J. Dunham. Vadose pisolite in the Capitan Reef (Permian), New Mexico and Texas. *SEPM Special Publication: Depositional Environments in Carbonate Rocks*, 14:182–191, 1969.

[55] M. Esteban. Vadose pisolite and caliche. *AAPG Bulletin*, 60(11):2048–2057, 1976.

[56] C.C. Kendall and J. Warren. A review of the origin and setting of tepees and their associated fabrics. *Sedimentology*, 34:1007–1027, 1987.

[57] A.F. Embry. The carbonate clastic cycles of the east-Alpine Raibl Group - result of 3rd-Order sea-level fluctuations in the Carnian - a discussion. *Sedimentary Geology*, 76(1-2):111–112, 1992.

[58] A.F. Embry and E.P. Johannessen. TR sequence stratigraphy, facies analysis and reservoir distribution in the uppermost Triassic-Lower Jurassic succession, western Sverdrup Basin, Arctic Canada. pages 121–146. 1992.

[59] T. Playton. Characterization, variations, and controls of reef-rimmed carbonate foreslopes. *Ph.D. Thesis*, University of Texas, Austin, 2008.

[60] C. Summa. *Sedimentologic, stratigraphic, and tectonic controls of a mixed carbonate-siliciclastic succession: Neoproterozoic Johnnie Formation, southeast California*. Ph.D. thesis, 1993.

[61] F.A. Corsetti and A.J. Kaufman. Stratigraphic investigations of carbon isotope anomalies and Neoproterozoic ice ages in Death Valley, California. *Geological Society of America Bulletin*, 115(8):916–932, 2003.

[62] M.E. Clapham and F.A. Corsetti. Deep valley incision in the terminal Neoproterozoic (Ediacaran) Johnnie Formation, eastern California, USA: Tectonically or glacially driven? *Precambrian Research*, 141(3-4):154–164, 2005.

[63] C.R. Calver. Isotope stratigraphy of the Ediacaran (Neoproterozoic III) of the Adelaide Rift Complex, Australia, and the overprint of water column stratification. *Precambrian Research*, 100(1-3):121–150, 2000.

[64] C. Kerans and S. Tinker. Extrinsic stratigraphic controls on development of the Capitan Reef. *SEPM Special Publication: Geologic Framework of the Capitan Reef*, 65:15–36, 1999.